HHS Public Access

Author manuscript

ACS Biomater Sci Eng. Author manuscript; available in PMC 2021 May 19.

Published in final edited form as:

ACS Biomater Sci Eng. 2020 March 09; 6(3): 1690–1703. doi:10.1021/acsbiomaterials.9b01837.

Porcine Vocal Fold Lamina Propria-Derived Biomaterials Modulate TGF-β1 Mediated Fibroblast Activation In vitro

Camilo Mora-Navarro[†,‡], **Andreea Badileanu**[†,‡], **Ana M. Gracioso Martins**[†,‡], **Emily W. Ozpinar**[†,‡], **Lewis Gaffney**[†,‡], **Ian Huntress**[§], **Erin Harrell**[§], **Jeffrey R. Enders**[⊥], **Xinxia Peng**[§,#], **Ryan C. Branski**[‖], **Donald O. Freytes**[†,‡,*]

[†]Joint Department of Biomedical Engineering, North Carolina State University/ University of North Carolina-Chapel Hill, Raleigh, NC

[‡]Comparative Medicine Institute, North Carolina State University, Raleigh, NC

[§]Department of Molecular Biomedical Sciences, North Carolina State University, Raleigh, NC

[⊥]Molecular Education, Technology and Research Innovation Center, North Carolina State University, Raleigh, NC

[#]Bioinformatics Research Center, North Carolina State University, Raleigh, NC

[‖]NYU Voice Center, Department of Otolaryngology–Head and Neck Surgery, New York University School of Medicine, New York, NY

Abstract

The vocal fold lamina propria (VFLP), one of the outermost layers of the vocal fold (VF), is composed of tissue-specific extracellular matrix (ECM) proteins and is highly susceptible to injury. Various biomaterials have been clinically tested to treat voice disorders (e.g., hydrogels, fat, hyaluronic acid), but satisfactory recovery of the VF functionality remains elusive. Fibrosis or scar formation in the VF is a major challenge, and the development and refinement of novel therapeutics that promote the healing and normal function of the VF are needed. Injectable hydrogels derived from native tissues have been previously reported with major advantages over synthetic hydrogels, including constructive tissue remodeling and reduced scar tissue formation. This study aims to characterize the composition of a decellularized porcine VFLP-ECM scaffold and the cytocompatibility and potential anti-fibrotic properties of a hydrogel derived from VFLP-ECM hydrogel. In addition, we isolated potential matrix-bound vesicles (MBVs) and macromolecules from the VFLP-ECM that also downregulated smooth muscle actin *ACTA2* under TGF-β1 stimulation. The results provide evidence of the unique protein composition of VFLP-ECM and the potential link between the components of VFLP-ECM and the inhibition of transforming growth factor-beta 1 (TGF-β1) signaling observed *in vitro* when transformed into injectable forms.

[*]Contact Author: Donald O. Freytes, Ph.D., Joint Department of Biomedical Engineering, North Carolina State University, University of North Carolina-Chapel Hill, 4208D Engineering Building III, Campus Box 7115, Raleigh, NC 27695, dofreyte@ncsu.edu, dfreytes@unc.edu, Office: +1 919-513-7933.

Supporting Information

The data file from the discovery proteomic performed is attached as a separate file.

The raw RNA-seq data have been deposited into NCBI GEO under the accession number GSE125463.

Graphical Abtract

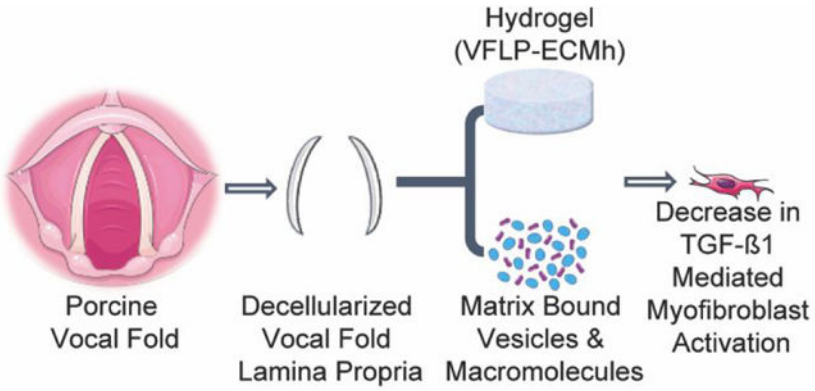

Keywords

Extracellular Matrix; Hydrogels; Vocal Fold Lamina Propria; MBVs; Fibrosis

1. INTRODUCTION

The vocal folds (VFs) are, arguably, the most mechano-active organ in the body. The simple act of phonation subjects the vocal folds to profound stress, strain, and compressive forces.[1] As such, the architecture of the VFs is impressive and engineered to withstand significant trauma.[2] However, repeated supra-threshold trauma and/or a myriad of potential sources of injury can yield substantive alterations to the tissue phenotype resulting in altered phonatory physiology, leading to diminished voice quality.[3] One of the most clinically challenging scenarios involves fibrosis or scarring of the VFs.[4] Of note, voice disorders are the most common communication disorder,[5] with nearly 20 million Americans reporting a voice disorder annually[6–7] at an annual cost comparable to conditions such as chronic obstructive pulmonary disease and asthma.[8–9] Beyond the financial costs, patients experience limitations in occupational and social function, lost income, and often report depression and anxiety.[10–12]

Fibroblasts are the main cellular component of the VFLP followed by myofibroblasts and macrophages.[13] Fibroblasts are critical for extracellular matrix (ECM) metabolism and are a potential therapeutic target given their putative role in vocal fold fibrosis. Prolonged fibroblast activation to the myofibroblast phenotype and its accumulation leads to aberrant overproduction of ECM-proteins and scar formation, thus altering the local protein tissue composition and function.[14–15] VFLP is a layered tissue composed of ECM proteins and polysaccharides such as elastin, collagen, glycosaminoglycans, and proteoglycans.[13, 16–18] The VFLP is further delineated into three layers: superficial, intermediate, and deep layers. The superficial VFLP is subjected to the most significant forces and is also the most common site of injury and subsequent fibrosis.[16, 19] Current therapies targeting VF scarring fail to recover function and primarily focus on tissue augmentation to improve VF closure. A full and functional VFLP replacement is challenging, given the significant variability in both ECM content and biomechanical properties specific to each individual. Approaches to VFLP

replacement with synthetic materials do not appear to be clinically viable, leaving a wide range of patients without options for regenerative therapy.[20–22] VF injury triggers the release of a variety of cytokines and signaling cascades aimed at promoting tissue recovery in which transforming growth factor β1 (TGF-β1) represents a major player during fibrosis. Since the fibrotic response alters the local protein composition affecting the function of the VFs, methods such as cryotherapy, PEG, and cell therapies have been used to target TGF-β1 signaling to enhance VF wound healing.[23–25] Nevertheless, current biomaterials and therapeutic approaches fail to capture the specific composition of VF tissue or have limited ability to modulate inflammatory and fibrotic responses underlying scar formation and altered VF function[22].

Generally, the transition of fibroblast to myofibroblast can lead to tissue fibrosis, which is characterized by aberrant ECM production and deposition.[26] Altered ECM deposition in the VFs has a direct, functional impact on tissue pliability and ultimately function. Ideally, a natural host degradable biomaterial-based therapeutic approach could promote a favorable physiological outcome that modulates scar formation and promotes the regeneration of functional VF tissue. Scaffolds derived via the decellularization of porcine tissues have emerged for clinical use or in preclinical studies due to wide availability, low immunogenicity, and inherent bioactivity.[27–30] ECM-scaffolds are naturally derived materials composed of mostly proteinaceous and non-proteinaceous components such as collagen, elastin, laminin, glycosaminoglycans, hyaluronic acid, fibronectin, and vitronectin.[31] ECM-scaffolds are biologically active and have been shown to promote pro-healing responses and suppress pro-inflammatory responses.[32–34] Furthermore, decellularized ECM scaffolds can be manipulated into a hydrogel form that is amenable for delivery to the site of injury *via* minimally invasive methods.[35] As an example, Ventrigel™ is a porcine-derived ECM-hydrogel that passed an FDA phase 1 clinical trial and exemplifies the potential of ECM hydrogels for use in a clinical settings.[36]

Our group previously described an efficient decellularization protocol for the derivation of porcine vocal fold-lamina propria extracellular matrix (VFLP-ECM).[27, 37] Our current goal was to derive and characterize injectable forms of the VFLP-ECM with potential anti-fibrotic effects on resident vocal fold fibroblasts, ultimately modulating scar tissue formation after material resorption. The present study is the first step towards the *in vitro* characterization of two potential injectable forms isolated from VFLP-ECM. We hypothesized that a VFLP-ECM hydrogel (VFLP-ECMh) will have anti-fibrotic properties by modulating TGF-β1 mediated fibroblast activation. We also hypothesized that these effects will be related to the presence of macromolecules and/or matrix-bound nanovesicles (MBVs) within the ECM that can also be used as injectable materials. The development of a biocompatible and anti-fibrotic injectable form of VFLP-ECM represents an essential step towards a regenerative and clinically transferable approach for vocal fold repair.

2. Experimental Section

2.1 Materials

Porcine vocal fold tissue and urinary bladders were obtained from the local market (Nahunta, Raleigh, NC). Primers were purchased from Integrated DNA Technologies

(Coralville, IA). Transforming growth factor beta-1 (TGF-β1), for activating fibrosis via the TGF-β1 pathway was purchased from Peprotech (Rocky Hill, NJ).

2.2 Tissue Dissection and Decellularization

Dissection and decellularization of the porcine VFLP was performed as previously described[37]. Briefly, the larynges were cleaned of connective tissue and frozen at −80°C for at least 48 hours. Larynges were then bisected and the lamina propria of each of the true vocal folds isolated. The VFLPs were then rinsed three times for 15 minutes in 1X DPBS and washed for two hours with sodium deoxycholate (4% w/v, Sigma-Aldrich, St. Louis, MO) and deoxyribonuclease (DNase) I (273 Kunitz mL^{-1}, Sigma-Aldrich), respectively, with 15-minute washes using 1X DPBS in between. Finally, a 30-minute wash in peracetic acid (0.1% v/v, Sigma-Aldrich) was followed by a final wash in 1X DPBS. Washed VFLPs were stored in 1X DPBS with penicillin/streptomycin (1% v/v, Life Technologies, Carlsbad, CA) at 4 °C. At this point, the scaffold was named VFLP-ECM. Similarly, urinary bladders were mechanically cleaned from connective tissue and decellularized as previously described[35].

2.3 Hydrogel Preparation and Gelation Kinetics

VFLP-ECM was frozen in liquid nitrogen and micronized using a mortar and pestle. The VFLP-ECM powder was collected in a 50 mL conical tube and lyophilized overnight. 100 mg of the lyophilized ECM was then digested with pepsin (6 mg, 3200–4500 units mg^{-1}; Sigma-Aldrich) in hydrochloric acid (10 mL, 0.01 M) for 48 hours on a magnetic stirrer at room temperature resulting in a digested ECM solution of 10 mg of ECM mL^{-1} [35]. The resulting pH of the digested ECM was 3–4; 0.9 mL aliquots were stored at −20 °C until use. VFLP-ECM hydrogels (VFLP-ECMh; 6 mg mL^{-1}) were prepared by thawing the digested VFLP-ECM on ice, neutralizing its pH with NaOH (0.1 M, Sigma-Aldrich), and balancing the salt content using 10X DPBS (6.7% v/v) and 1X DPBS (27.5% v/v). Once the pH tested neutral (7.3 +/− 0.2), 400 μL of either VFLP-ECMh, UBM-ECMh, or Col. 6 mg mL^{-1} were pipetted into each well of a 24-well plate (Corning, Corning, NY). The plate was heated at 37 °C for 45 minutes to allow the VFLP-ECMh to crosslink into a gel. For gelation kinetics, VFLP-ECMh and Collagen type I hydrogel (Col.) at 6 mg mL^{-1} (FibriCol I, Collagen Type I >97%, Advanced Biomatrix, Carlsbad, CA) were distributed at 100 μL per well at least in triplicates in a 96-well plate and kept on ice until measurement in a BioTek SYNERGYneo2 multimode reader pre-heated to 37 °C. Absorbance measurements were taken at 405 nm every 1 minute for 1.5 hours. Each precursor gel solution had a different absorbance at 405 nm and the minimum absorbance was selected as reference (A_0), which was different between the hydrogels. The procedure for data normalization and analysis is provided in the supporting information (Equation A.1).

2.4 Scanning Electron Microscopy (SEM)

Surface morphology of the VFLP tissue, VFLP-ECM powder, and VFLP-ECMh was evaluated using SEM or CryoSEM on a JEOL JSM-7600 FE SEM (JEOL USA, Peabody, MA) equipped with Alto-2500 (Gatan, Warrendale, PA). VFLP-ECMh at 6 mg mL^{-1} ECM concentration was mounted to a cooling holder and transferred to a super-cooled liquid nitrogen slush for cryopreservation. Once cooled, the sample was transferred under vacuum

to the Alto-2500 preparation chamber. The sample was then fractured using the attached scaffold knife. Next, the fractured sample was etched at −95 °C under 4×10^{-6} mbar vacuum for 5 minutes to remove ice crystals. After etching, the sample was allowed to cool to −120 °C and sputter-coated with gold/palladium alloy at 5nm thickness before transfer to the microscope cold stage for imaging. Lyophilized VFLP-ECM powder was mounted onto an adherent tape, placed on a holder, and transferred under vacuum to the Alto-2500 preparation chamber. Next, the sample was sputter-coated under the same conditions as previously described and moved to the microscope stage for imaging.

2.5 Atomic Force Microscopy

The local surface modulus of VFLP-ECMh and collagen hydrogels were determined using atomic force microscopy (AFM) (Asylum MFP-3D Bio, Asylum Research, Santa Barbara, CA, USA) in contact force mode using polystyrene cantilevers with chromium/gold coating (NanoAndMore, Watsonville, CA, USA). The cantilevers had a particle diameter of 6.1 μm. The spring constant of each cantilever was determined using the AFM software (Igor Pro 15). Force maps (10 μm × 10 μm) were collected for VFLP-ECMh and Col. at 6 mg mL^{-1}. Three hydrogels were analyzed per group with a minimum of three force maps consisting of 256 force curves each per hydrogel. The Hertz model was used to fit each force map in order to obtain Young's modulus.

2.6 Human Vocal Fold Fibroblast cell culture conditions

A human vocal fold fibroblast cell line produced by the Branski Laboratory, referred to as HVOX, was employed in the current study.[1] A primary cell line Human Dermal Fibroblast neonatal (HDFn, ATCC® PCS-201–010) was used for the transcriptomic assay. HVOX and HDFn were cultured in tissue culture plastic flasks and maintained in Dulbecco's Modified Eagle Medium (DMEM) (Life Technologies) with 10% fetal bovine serum heat-inactivated (Genesee Scientific, San Diego, CA) and 1% penicillin/streptomycin. The media was replaced every 3 days. Cell passages 7–15 were used for this study; HVOX were passaged by incubating with trypsin-EDTA (0.25%, Life Technologies) for 5 minutes and seeding onto tissue culture plastic flasks (VWR, Radnor, PA).

2.7 HVOX Viability and DNA isolation

Cell viability was analyzed using the LIVE/DEAD Viability/Cytotoxicity Kit for mammalian cells after 3 days on VFLP-ECMh (ThermoFisher Scientific) according to the manufacturer's instructions. Double strand DNA was quantified using the Quant-iT™ PicoGreen™ dsDNA Assay Kit (Thermo Fisher Scientific).

2.8 RNA Isolation and Real Time Quantitative Polymerase Chain Reaction

Samples were collected in 350 μL of TRK Lysis Buffer supplied with the E.Z.N.A. Total RNA Kit I (Omega Bio-tek, Norcross, GA) and stored at −80 °C. The 3-D culture samples were homogenized in lysis buffer using a bead mill 24 homogenizer (Fisher Scientific) and 1.4 mm ceramic bead media (ThermoFisher Scientific). RNA was then isolated according to the manufacturer's instructions. mRNA was retrotranscribed into cDNA Using the GoScript™ Reverse Transcription System (Promega, Madison, WI) according to the

manufacturer's instructions, and then real-time quantitative polymerase chain reaction (RT-qPCR) was performed on the QuantStudio 3 Real-Time PCR System (ThermoFisher Scientific) using SYBR Green (ThermoFisher Scientific). Table S1 lists all the forward and reverse sequences for RT-qPCR[38]. Glyceraldehyde 3-phosphate dehydrogenase (GAPDH) was used as the housekeeping gene.

2.9 Cell Seeding and TGF-β1 myofibroblast activation

2.9.1 2-D culture experiments—VFLP-ECM and Col. (6 or 4 mg mL^{-1}) were prepared and poured into 24 well plates for 40–60 minutes at 37 °C. HVOX at 70% confluence were detached and counted. HDFn were cultured under similar conditions. 4×10^4 cells were seeded onto each hydrogel condition and 1×10^4 cells on Tissue Culture Plastic (TCP) as a control. Cells were allowed to attach during overnight incubation. TGF-β1 [10 ng mL^{-1}] in media was used as the stimulus to induce myofibroblast activation. The media was replaced with fresh media in untreated conditions. Cells were treated for 48 hours and either lysed for RNA isolation (section 2.8) or fixed depending on the subsequent experiments.

2.9.2 3-D culture experiments—VFLP-ECMh, Col. 6 mg mL^{-1}, and UBM-ECMh were prepared and homogeneously mixed with HVOX at a cell density of 1000 cells μL^{-1} gel and cured in the incubator at 37 °C for 40 minutes. The media was added after gel formation and left in the incubator overnight. TGF-β1 [10 ng mL^{-1}] in media was used as the stimulus to induce myofibroblast activation. Untreated conditions received only media. Cells were treated for 48 hours and lysed for RNA isolation (see 2.8 section).

2.10 Transcriptome Analysis

Total RNA was purified from cell pellets using the miRNeasy extraction kit (Qiagen) according to the manufacturer guidelines. RNA quality was assessed on the Bioanalyzer 2100 instrument using RNA 6000 Nano Kit (Agilent). mRNA-seq sequencing libraries were prepared from 1μg purified RNA using Illumina's TruSeq Stranded mRNA Library Prep Kit. Deep sequencing was performed on a Nextseq500 sequencer (Illumina) using 75bp paired-end reads. Raw BCL (base call) files generated from NextSeq sequencer were converted to FASTQ files using bcl2fastq Conversion Software v2.18. During BCL to FASTQ processing, bcl2fastq also separates multiplexed samples, removes adapters, trims low-quality bases, and removes low-quality reads. Raw RNA-seq data in FASTQ file format was quality controlled during and after sequencing to identify potential technical issues. Raw sequencing reads were mapped to the human reference genome (assembly GRCh38, Gencode annotation release 29) using STAR[39] to generate read counts for each of the annotated genes. Gencode transcript annotations were supplied to facilitate the mapping of reads spanning known splicing junctions. For differential expression analyses, only those genes with more than 50 raw read counts in at least two biological samples in both cell types were included. Raw gene read count data were normalized using the voom approach[40]. Differential expression analysis was performed using the linear model approach provided by the limma package[40–41]. The p-values for the coefficient/contrast of interest were adjusted for multiple testing the Benjamini and Hochberg's method[42], to control for expected false discovery rate (FDR). The significance threshold for gene differential expression was defined as fold

change greater than two and FDR less than 0.05. Functional enrichment analysis of predicted regulators and molecular pathways was performed using QIAGEN's Ingenuity Pathway Analysis (Redwood City, CA). The raw RNA-seq data have been deposited into NCBI GEO under the accession number GSE125463.

2.11 ACTA2 and COL1A1 expression in HVOX

HVOX were cultured on TCP, VFLP-ECMh, and Col. and then stimulated with TGF-β1 for 48 hours, as described for myofibroblast activation. After TGF-β1 exposure, the cells were lysed, and total RNA was isolated to evaluate *ACTA2* and *COL1A1* expression using RT-qPCR.

2.12 ACTA2 protein (α-SMA) immunostaining

After 48 hours of TGF-β1 stimulation as described in **2.10,** cells were fixed with 2% formaldehyde (diluted in media) and then 4% diluted in DPBS. Then, fixed cells were then permeabilized with 0.1% Tween-20 (diluted in DPBS 1X; Sigma Aldrich) and blocked overnight in 1% bovine serum albumin (ThermoFisher Scientific) at 4°C. After overnight incubation, the cells were briefly washed and treated with anti-smooth muscle actin conjugated antibody at 2 μg mL^{-1} (Alexa Fluor 488, ThermoFisher Scientific) overnight at 4°C and treated with ReadyProbes DAPI (Life Technologies) for 5 minutes at 25°C. Cells were washed with 1X DPBS after each treatment, and the plate wrapped with parafilm, covered with aluminum foil, and stored at 4°C until imaging. Cells were imaged using a Zeiss LSM 710 or a FluoView 3000 FV3000 Olympus confocal microscope. Laser intensity was adjusted per material (i.e., TCP, VFLP-ECMh, UBM-ECMh, or Col. 4 or 6 mg mL^{-1}) until saturation was reached using the TGF-β1 treated cells as a reference with constant voltage for each material (TGF-β1 treated or untreated). Images were acquired using Zeiss and then processed using ImageJ. FluoView software was used to process the images from the FV3000. The experiments were repeated at least six independent times.

2.13 Proteomic Analysis

Digestion: 2–3 mg of decellularized and micronized VFLP-ECM and UBM-ECM samples (n=3) were suspended in 1 mL of 50 mM ammonium bicarbonate (pH 8.0) with 5% Sodium Deoxycholate (SDC) for digestion and determination of their protein concentration, see further methodology details in Proteomic Method S1.

Nanoflow Liquid Chromatography: All samples were processed according to a discovery proteomics workflow using a quadrupole orbitrap (Q Exactive HF, Bremen Germany). PicoFrit® columns were purchased from New Objective (Woburn, MA) and packed to a length of 20–30 cm with reverse-phase ReproSil-Pur 120 C-18-AQ, 3 μm particles (Dr. Maisch, Germany). Orbitrap Mass spectrometry: Orbitrap tandem mass spectrometry was performed using a Thermo Scientific Q-Exactive HF (Bremen, Germany) in a top 20 data-dependent acquisition mode (DDA), where the 20 most abundant precursors were selected for fragmentation per full scan. Samples were run in random order, and a quality control bovine serum albumin (BSA) digest was run every fifth injection to ensure proper LC-MS/MS reproducibility.

- Data Analysis: Proteome Discoverer 2.4.0.305 was used for analysis
- A label-free quantitation (LFQ) workflow was used
- Resulting "Abundances (Scaled)" can be used for *relative quantitation*
- SwissProt (reviewed proteins only) and TrEMBL (unreviewed proteins only) for Sus Scrofa (taxonomy ID = 9823) were used for peptide searching
- Max of 8 equal mods and max of 3 total dynamic mods per peptide

2.14 Matrix-bound nanovesicles isolation

Decellularized VFLP-ECM was resuspended at 5 mg mL^{-1} in the digestion buffer according to the protease. VFLP-ECM was digested for 48 hours using either Collagenase Type II (collagenase II) (ThermoFisher Scientific, at 0.2 mg mL^{-1} in Tris base-pH 8.0 (50 mM), NaCl (0.2 M), CaCl2 (5 mM), MgCl2 (0.5 mM) or Proteinase K (MilliporeSigma, 0.1 mg mL^{-1}) in Tris-HCl (50 mM), NaCl (200 mM) buffer. The Proteinase K digestion product was used for particle characterization and the collagenase II digestion product was used for both particle, and biological characterization. After digestion, the samples were centrifugated sequentially at 500, 2500, and 10000 g-force for 30 minutes each to remove debris from ECM-like fibers remaining in suspension. MBVs were isolated and concentrated using an ultrafiltration protocol, as previously described[44–46]. The final digested product was concentrated using an Amicon®Ultra-15 100kDa membrane (MilliporeSigma) following the manufacturer instructions and washed once by adding 8mL DPBS 1X yielding 250 μL of concentrated solution. The concentrated volume was increased to 1 mL with fresh DPBS 1X, aliquoted, and stored at −80 °C until characterization preparation.

2.15 Particle characterization by Transmission Electron Microscopy (TEM) and Nanoparticles Tracking Analysis (NTA)

MBVs were isolated three independent times, and the extract was characterized using TEM imaging. 10 μL samples digested via Proteinase K or collagenase II were negatively stained using Uranyl Acetate and images were taken with a Talos F200X G2, 200 kV FEG (Field Emission Gun), Analytical Scanning Transmission Electron Microscope (S/TEM). MBV size was characterized in PBS (pH= 7.4) using a Malvern NanoSight NS300 (Malvern Instruments, Worcestershire, UK) to determine particle hydrodynamic radii, size distribution, and particle concentration. The analysis was performed using five video measurements of 30 seconds each. The gain was set to three, and the threshold was two.

2.17 Biological effect characterization of macromolecules and MBVs isolated from VFLP-ECM

NTA analysis was used to estimate the particle concentration of MBVs and other potential macromolecule products larger than 100 KDa. Particle concentration to supplement cell culture media (i.e., DMEM + 10% FBS-HI + 1% P/S) was set to 25,000 particles μL^{-1}. HVOXs between 70–90% confluence were detached using trypsin 0.05%, counted, and cultured in a 24-well plate at a cell density equal to 4000 cells cm^{-2}. Cells were seeded and incubated overnight in two media conditions: (1) cell culture media, and (2) cell culture media supplemented with MBVs. Following an overnight incubation to allow HVOX to

attach, media and MBV supplemented media were replaced with fresh media, fresh MBV supplemented media, media+TGF-β1 [10 ng mL^{-1}], and TGF-β1+MBV supplemented media for 48 hours. *ACTA2* mRNA expression was analyzed as described in section 2.12.

2.16 Statistics

Student t-test was performed for paired observations; $p<0.05$ was considered statistically significant for *ACTA2* and *Col1A1* expression in at least three independent experiments. Statistical analysis was performed using GraphPad PRISM 8.0 software. All experiments were independently replicated at least three times unless otherwise noted.

3. Results

3.1 Overall approach

Developing a new injectable biomaterial capable of modulating the wound healing response in VF tissue represents a challenge mainly due to the unique protein, non-proteinaceous composition, and material properties of the VFs.[47] Following injury, fibroblasts (among other cells) play an essential role during the wound healing process. Fibroblast activation towards a myofibroblast phenotypes is often associated with scar formation, which compromises VF functionality. Scar formation is associated with overproduction and deposition of ECM proteins such as collagen leading to altered tissue architecture and aberrant function. Current technologies proposed to restore the function of the VFs largely fail to modulate critical pathways associated with fibrosis or enhance anti-fibrotic activities.[22] The current study describes the characterization of two injectable forms of the VFLP-ECM, a hydrogel and MBVs, and focuses on the characterization of its *in vitro* properties and their effect on myofibroblast activation via TGF-β1.

Figure 1 provides a schematic of the overall approach. First, VFLP (native) was dissected from porcine larynges. Each batch of decellularized VFLP was processed using at least 20 dissected tissues representing a biological pool from 10 animals. As a first step, VFLP were decellularized and micronized into a powder form which constitutes the raw material. VFLP-ECM was characterized via proteomic analysis and compared to a commercially available ECM-scaffold. Decellularized VFLP-ECM powder was then enzymatically digested and turned into a hydrogel (VFLP-ECMh). The physical and TGF-β1 modulation properties of the VFLP-ECM hydrogel were then tested in vitro. Collagen type I hydrogel (Col.) was used as a control due to its extensive use in VF treatment when compared to other collagen types.[48] In addition, matrix-bound vesicles (MBVs) and macromolecules larger than 100 KDa were isolated from the digested VFLP-ECM and tested for TGF-β1 mediated activation of fibrosis. This study represents the first derivation and characterization of a VFLP-specific hydrogel with anti-fibrotic properties.

3.2 VFLP-ECM decellularized and hydrogel characterization

Figure 2A shows macroscopic (top panels) and scanning electron micrograph images (bottom panel) of the different forms of VFLP-ECM. Decellularized VFLP-ECM is shown in Figure 2Ai, VFLP-ECM had a final DNA concentration of 4 μg mg^{-1} dry tissue +/−1.3.

Multiple VFLP-ECMs were micronized and mixed to create a powder form of the VFLP-ECM (Figure 2Aii).

The powder form was then digested and polymerized, as shown in Figure 2Aii. Following decellularization, VFLP became a clear-white biomaterial as presented in Figure 2A, I; micrograph IV shows dense fibril-like ECM structures with some degree of organization (no cells were identified in any images). SEM images (Figure 2AV) consistently showed an irregular surface for this type of scaffold.

To characterize the self-assembly kinetics of the hydrogel, gelation kinetics was quantified by measuring changes in turbidity for VFLP-ECMh and compared to other hydrogels at 6 mg mL^{-1} such as Col., and UBM-ECMh (Figure 2B). The plot shows a sigmoidal-gelation behavior for the VFLP-ECMh with a gelation speed (S) of 0.04 min^{-1} where t_{lag}= 24 min ± 2.3, t_{50}=34.5 min ± 1.3, and t_{95}=50 min ± 2.

Complex viscosity was compared between VFLP-ECMh to Col. (see appendix, Figure S1i). Under the frequencies tested, VFLP-ECMh was relatively similar to Col. except between 0.1–1.0 Hz, where a minor deviation in complex viscosity were observed[49]. However, these differences can be explained by batch-to-batch variability. Table S2 summarizes the complex viscosity curve using Equation S2–3. The estimated k values resulting from Linear Least-Squares Regression Curve-Fitting suggest that VFLP-ECMh is less viscous than Col.[50] Table S2 also lists the parameters from the Equation S3 for other hydrogel materials with potential use in VF treatment. The values listed in Table S.2 were used for comparison only since the mechanical properties of the VFLP-ECMh are anticipated to rapidly change following delivery due to the resorption of the material as a result of the host tissue response.[51–52]

At a cellular level, the mechanical properties of ECMh can influence the initial biological response (e.g., fibrosis, development, tissue homeostasis, wound healing, etc.), and therefore, the “cell-level” stiffness of VFLP-ECMh was examined (Figure 2C) using atomic force microscopy (AFM).[53] AFM was used to determine the local elastic modulus of VFLP-ECMh and Col. at a concentration of 6 mg mL^{-1}. Viscoelastic characterization via AFM showed that collagen had a lower but not statistically significant modulus than VFLP-ECMh (modulus (Pa): Collagen=143.4 ± 35.0, VFLP-ECMh=152.5 ± 34.7, and UBM-ECMh=137.2 ± 17.2; $p>0.05$ (i.e., n.s.)). Figure 2Civ is a representative 10×10 μm area force map from VFLP-ECMh. The plot presents a conservative variance in the changes in the local force of the material surface. UBM-ECMh data are presented in the supporting information Figure S1ii with a modulus mean of 137.2 ± 17.2 Pa, similar to VFLP-ECMh.

Figure S1iii shows the cytocompatibility of VFLP-ECMh using LIVE/DEAD staining showing a high number of live HVOX on VFLP-ECMh. The green signal allowed for visualization of elongated, spindle-shaped morphology characteristic of cells proliferating on VFLP-ECMh. This morphology was expected for these cells on hydrogel materials. Figure S1iv shows the quantity of DNA isolated from cells cultured on VFLP-ECMh or Col. suggesting proliferation in both materials.

3.3 TGF-β1 Mediated Fibrotic Activation

Fibroblasts are key players in wound healing in a variety of tissues, and the vocal folds are no exception. Vocal fold fibroblasts readily activate to myofibroblasts in response to TGF-β1. Activated myofibroblasts promote scar formation due to the overproduction and deposition of many ECM proteins.[4, 54–55]

To understand the overall biological impact of VFLP-ECMh at the molecular level, we performed transcriptome deep sequencing (RNA-seq) analysis of HVOX and HDFn cultured on tissue culture plastic (TCP), VFLP-ECMh, and Col. with or without TGF-β1 stimulation. For simplicity, TGF-β1 treated groups were marked by an asterisk (e.g., VFLP-ECMh* represents a group seeded with cells on VFLP-ECMh and treated with TGF-β1 at 10 ng mL^{-1}). The combination of the stiffer surface in the TCP (mechanical stress) and TGF-β1 (cytokine phenotype induction) elicited a myofibroblast phenotype, which was used as a positive control.[14] Fibroblasts in Col. 6 mg mL^{-1} provided a microenvironment with stiffness comparable to VFLP-ECMh, allowing for the evaluation of the impact of the material on TGF-β1-mediated activation.

The heat map in Figure 3A shows that many annotated TGF-β1 targeted genes were down-regulated in cells seeded on VFLP-ECMh alone, indicating that VFLP-ECMh had a direct impact on TGF-β1 target genes. In comparison, gene expression differences were less pronounced in cells cultured on collagen. In Figure S2i, expression profiles of HVOX cells cultured on VFLP-ECMh* versus TCP* are provided to illustrate how the ECM affected TGF-β1 signaling. As expected, TGF-β1 induced substantial gene expression changes in HVOX. Of note, these gene expression patterns were reduced or even reversed in cells seeded on VFLP-ECMh and stimulated with TGF-β1, as shown by the red trend line in Figure S2i.

Figure 3B represents a functional study of the differentially expressed genes significant for the analysis (Z score and −Log (p)value). The analysis showed that the activation of TGF-β1 target genes was overall reduced (green color for VFLP-ECMh condition). The data suggest that VFLP-ECMh may directly inhibit some of the effects of TGF-β1 treatment on fibroblasts. A second differential analysis was performed to measure global expression changes induced by each of the three biomaterials in HDFn and HVOX (Figure S2ii). In summary, similar expression changes were observed in both cell types grown on VFLP-ECMh compared to cells grown on TCP without TGF-β1 stimulation (Figure S2iii). Additionally, the effects of VFLP-ECMh were not unique to HVOX; similar data were obtained for HDFn (Figure S2iii).

The transcriptome showed downregulation of the *ACTA2* gene for HVOX cultured on VFLP-ECMh, which is a hallmark for the myofibroblast-like phenotype; therefore, we used RT-qPCR to measure its expression level under 3-D culture conditions. Figure 3C shows that the *ACTA2* expression level was not different in HVOX cultured within VFLP-ECMh or VFLP-ECMh upon TGF-β1 treatment. The result was compared to the upregulation of ACTA2 expression by HVOXs cultured within Col. following TGF-β1 treatment as a positive control. The lack of any change in *ACTA2* expression of HVOXs cultured within

VFLP-ECMh may suggest a modulatory response of HVOXs when cultured in 2-D or 3-D conditions.

The modulatory effects of VFLP-ECMh were also confirmed via immunostaining for α-SMA, as shown in Figure 3D and Figure S3. Baseline expression of α-SMA was expected in fibroblasts. However, myofibroblast activation results in increased contractile forces, cell morphology changes, and scar tissue formation, which are directly related to *ACTA2* expression and incorporation of *ACTA2* into cytoskeletal filaments.[15] Figure 3D shows representative images of α-SMA staining. Expression of α-SMA increased in HVOX cultured on TCP and collagen (Figure S3) in response to TGF-β1. In contrast, α-SMA expression did not increase in HVOX cultured on VFLP-ECMh treated with TGF-β1 (Figure 3Diii–vi). Intensity and distribution of α-SMA expression following TGF-β1 exposure were evaluated in untreated cells on the same material as baseline measurements. TGF-β1 treatment of cells seeded on TCP or collagen resulted in more defined cytoskeletal filaments, as shown in the immunostaining Figure 3Div and v, respectively. Increased expression was observed across two concentrations of collagen hydrogels (4 and 6 mg mL^{-1}) and in cells cultured on TCP (representative images were selected for Figure 3D and Figure S3). In contrast, α-SMA expression was not upregulated in HVOX cultured on VFLP-ECMh. These results are in agreement with the gene expression analysis.

3.4 Proteomic Comparison between Vocal Fold Lamina Propria and Urinary Bladder Derived ECM

Comprehensive proteomic discovery analysis was performed to characterize the tissue-specific microenvironment of the VFLP-ECM scaffold. The protein composition was contrasted against UBM-ECM (representative control of a commercially available ECM scaffold). Proteomic studies involved the identification and estimation of abundances of protein-based on peptide fragments produced after digestion of VFLP-ECM or UBM-ECM using trypsin, as described in section 2.13. Overall, the protein composition of the precursor and the hydrogel remained comparable regardless of the digestion method (e.g., pepsin in HCl 0.01 M or with trypsin).

The Venn diagram in Figure 4A illustrates the number of proteins identified: 1979 proteins for VFLP-ECM and 1655 for UBM-ECM. The comparison yielded 1430 commonly identified proteins. The analysis also revealed a higher number of proteins only found in the VFLP-ECM (549) when compared to proteins detected in UBM-ECM (255).

To further analyze VFLP-ECMh, we evaluated ECM-related proteins preserved in the two decellularized ECM scaffolds (VFLP and UBM). Protein abundance quantification was calculated using the Log2 of the fold change (FC) of the VFLP-ECM with reference to the UBM-ECM (see Supporting file_matrix29_ Perseus analysis_Volcano Plot). Figure 4B shows a volcano plot using a False Discovery Rate (FDR) equal to 0.01; the names of genes in the scheme correspond to selected ECM-related proteins with significant abundance in either of the scaffolds. A positive Log2 FC represents a higher abundance for proteins detected in the VFLP-ECM than those detected in UBM-ECM. Figure 4B shows the gene names of a cluster of glycoproteins (*LAMB1, LAMB2, and LAMA4*) as well as integrins (*ITGA1, ITGA3, ITGA5, ITGA7, ITGFB1, ITGFB3a*) with lower abundance in the VFLP-

ECM scaffold, excluding ITGB4 from the Integrins group, which was higher in VFLP-ECM relative to UBM-ECM.

VFLP-ECM analysis showed the presence of a variety of ECM-related proteins such as collagens, keratins, fibrillin, elastin, and proteoglycans; therefore, a hierarchical characterization of ECM-related proteins is shown in Figure 4C. The positive or negative symbol in parenthesis next to the gene name indicates if the abundance was significantly different or not compared to UBM-ECM. The heat map also shows ECM-related proteins detected in only one ECM scaffold, such as elastin (*ELN*), which was detected in VFLP-ECM only. In addition, the map shows the Log2 of the label-free quantification values (LFQ) of proteins for which the difference in abundance in the decellularized material was not significant.

Interestingly, *COL18A1* was detected in both ECMs, but without a significant change in the Log2 LFQ per replicate assayed. In addition, *EMILIN1* and *EMILIN2*, which are members of the EMILIN's family of three structurally homologous glycoproteins, were also detected in both biomaterials. GeneMANIA online application was then used to visualize potential association between the ECM-proteins shown/detected in the hierarchical analysis and the TGF-β1 myofibroblast activation pathway (Figure S4). The volcano plot obtained using a false discovery rate (FDR) of 0.01 (Figure 4D) highlights genes extracted from GeneMANIA analyses.

EMILIN1 was identified in both materials without showing statistical differences between the ECM scaffolds, with a Log2 LFQ abundance around 23, as depicted in the heatmap. Decorin (*DCN)* and Dermatopontin *(DPC)* were also identified, but the difference between scaffolds was not statically significant.

However, as shown in Table 1, LFQ values for *DCN* and *DPC* in the scaffolds were relatively higher (~Log2 LFQ 32). *CILP2* was also detected significantly in the VFLP-ECM and it is reported as highly homologous to *CILP-1.* Another interesting protein identified in a high relative abundance in VFLP-ECM was latent TGF-β1 binding protein (*LTBP4*), which may provide insight regarding tissue-specific cues in VFLP-ECM. These proteins were identified in the raw material of the hydrogel and MBVs derived in this study. However, the protein integrity in the injectable materials and its role in any response needs to be further investigated and will be the subject of future studies.

We evaluated the effects of VFLP-ECMh on myofibroblast activation by measuring *ACTA2* and *Col1A1* expression in HVOX cultured on VFLP-ECMh, UBM-ECM-h, and Col. via RT-qPCR. As expected, Col. condition resulted in an upregulation shifting trend in *ACTA2* and *Col1A1* expression in HVOX following TGF-β1 activation. For each condition tested, the biological reference was the basal gene expression of untreated cells seeded on its corresponding material. Error bars represent the standard error of the mean for at least four independent experiments. Figure 4E shows that cells grown on VFLP-ECMh+TGF-β1, and UBM-ECMh+TGF-β1 had similar *ACTA2* gene expression profiles. HVOX grown on Col.+TGF-β1 showed upregulation of *ACTA2* and *Col1A1. Col1A1* expression in cells cultured on VFLP-ECMh+TGF-β1 was significantly downregulated compared to UBM-

ECMh+TGF-β1. It is important to highlight that AFM confirmed that the elastic modulus across all tested hydrogel scaffolds was similar, suggesting that local mechanical properties were unlikely to contribute to gene expression.

The likely component of VFLP-ECM responsible for modulatory effects on fibroblast activation remains unknown. To further characterize the biologically active components of VFLP-ECM, a recently described approach to isolate matrix-bound nanovesicles (MBVs) and macromolecules larger than 100KDa from decellularized ECM was employed. MBVs provide an injectable agent that can also be used to modulate local host tissue response within injured VFs. Figure 5A describes the approach used to separate and concentrate MBVs using an ultrafiltration method for the enrichment of microvesicles and used for nanocarriers (e.g., exosomes).

The VFLP-ECM was digested using either Collagenase II or Proteinase K, as shown in Figure 5. A series of centrifugations were used to remove ECM-like fibers in suspension after digestion. Finally, a 100kDa membrane was used to ultra-filtrate the material keeping the MBVs and further macromolecules in the fraction unable to pass through the 100KDa membrane. Figure 5B shows representative transmission electron microscopy (TEM) images of samples from three different digestion batches. TEM revealed vesicle-like structures as a result of both digestion techniques, Collagenase II and Proteinase K, and ultrafiltration isolation (some pointed with the yellow arrows; 50– 200nm). Particle measurement via Nanoparticle Tracking Analysis (NTA) was performed. Figure 5C is a representative NTA analysis from a group of three independent experiments, which evidenced particle distribution aligned with TEM images (125–300nm). These data support the isolation of MBVs from decellularized VFLP-ECM using the ultrafiltration method but does not exclude the presence of macromolecules larger than 100KDa in the isolated product. The biological effect of this extract was tested using HVOX seeded on tissue culture plastic (TCP) and stimulated with TGF-β1. Figure 5D shows the fold change (FC) data for *ACTA2* expression. As expected, the positive control TCP+TGF-β1 did not modulate *ACTA2* expression, appearing around 5 times higher than the reference (HVOX untreated). Cells grown in media supplemented with MBV and macromolecules isolated from VFLP-ECMh displayed downregulation of *ACTA2*. Remarkably, cells supplemented with MBVs and stimulated with TGF-β1 showed a slight increment in the *ACTA2* expression; however, still significantly below the reference without supplementation or TGF-β1 treatment. RT-qPCR results were confirmed by α-SMA immunostaining, as shown in Figure 5E. Confocal imaging revealed altered morphology as well as α-SMA expression in cells grown without MBVs and treated with TGF-β1. No differences in the gene expression of HVOX were noted upon TGF-β1 treatment in cells grown in media supplemented with MBVs and macromolecules.

4. Discussion

Treatment of aberrant vocal fold phenotypes has primarily sought to augment the tissue by injecting biomaterials derived from different sources and compositions to enhance the wound healing process.[56–58] An ideal therapeutic should be amenable to delivery via injection under minimally invasive conditions and should promote constructive remodeling

while avoiding excessive scar tissue formation. The major goal of the present study was to derive and characterize injectable biomaterials from decellularized porcine vocal fold lamina propria. Hydrogels derived from a variety of materials (e.g., collagen Type I) have been injected into vocal folds to enhance healing, but without ameliorating regenerative outcomes.[59–61] Similarly, decellularized ECM laminar scaffolds derived from porcine liver or urinary bladder matrix (UBM-ECM) have been recently used to treat VFs have failed to modulate scar formation.[62–63] A hydrogel derived from the VFLP-ECM may provide an abundance of site-specific signals to modulate the fibrotic response and promote VF specific tissue remodeling. Initially, we sought to characterize the unique compositional properties of a decellularized VFLP-ECM and the ability of the injectable hydrogel form of VFLP-ECM (VFLP-ECMh) to modulate TGF-β1 mediated fibroblast activation. VFLP was decellularized using a recently published protocol, which only requires about 6 hours to yield an acellular ECM-scaffold maintaining critical ECM components.[27, 37] Reduced decellularization time has the added benefit of reducing the potential loss of important ECM components and maintaining the unique composition of the VFLP tissue.[29] The hydrogel form of the VFLP further allows clinicians to deliver the ECM to the site of VF injury via injection in an outpatient setting.

Gelation or self-assembly kinetics of VFLP-ECMh showed a moderate transition to hydrogel form with a t_{50}~34.5 min when compared to Col., which transition in approximately 30 minutes. This transition has been reported to be the result of the self-assembly of collagen like-fibers suggesting that the VFLP-ECMh kinetics could be driven by the presence of additional ECM components such as elastin, laminins, or proteoglycans.[35] The gelation kinetics profile for VFLP-ECMh was analogous to UBM-ECMh. This similarity is important because Col. and UBM-ECMh have been injected in VFs in previous studies. VFLP-ECMh had comparable visco-elastic behavior when contrasted to other injectable materials supporting the notion that decellularized VFLP-ECMh could offer a unique biomaterial in terms of composition and microenvironment with appropriate material properties that could be better suited for VF treatment.

To characterize potential anti-fibrotic effects on fibroblasts, characterization of mechanical properties of the hydrogel at a cellular level was needed. Previous studies showed that substrate stiffness could mediate myofibroblast activation where mechanical stress from stiffer cell culture materials such as TCP or glass elicited a proto-myofibroblast phenotype compared to cells grown on softer conditions such as hydrogels.[15] The elastic modulus from the different hydrogels tested was similar to reported values (100–300 Pa) for common ECM hydrogels at standard concentrations.[64–65] Also, the elastic moduli obtained were below the reported values known to activate fibroblasts *in vitro*, which further supports the use of VFLP-ECMh as a therapeutic agent.[66] In addition, the VFLP-ECMh had mechanical properties comparable with other scaffolds used for VF applications such as hyaluronic acids, alginates, and collagen type I.[22, 67] The local elastic modulus suggests no significant differences were observed between the hydrogels tested, which allow us to rule out any significant contributions by the substrate in terms of stiffness-driven effects upon TGF-β1 treatment to promote myofibroblast activation.

Given the ultimate goal of modulating fibrosis, our analysis focused on potential ECM-compositional proteins identified during the proteomic analysis on the raw material that might affect TGF-β1 related fibroblast activation if bioactivity surpass pepsin digestion processing. Further studies are necessary to identify if any biologically active matricryptic peptides remain in the residual cleavage protein/peptides in the VFLP-ECMh produced from the pepsin digestion of the VFLP-ECM.[68] Proteomic discovery detected different types of collagen in the VFLP-ECM; more specifically, the hydrogel material intrinsically preserved different ratios of native porcine collagen proteins compared to UBM-ECM. Among the collagens identified in VFLP-ECM, *Col18A1* may be particularly relevant due to a potential presence of Endostatin. Endostatin is a protease-derived peptide of *COL18A1* (matricryptin or matrikine, a product of ECM degradation), and if it remains active, it has been reported to modulate fibrosis in liver and lung models.[69] Gene association search identified specific proteins in the VFLP-ECM that correlate with the TGF-β1 pathway. *EMILIN1* was detected in the VFLP-ECM and is associated with the TGF-β1 antagonistic pathway.[70–74] Meanwhile, *EMILIN2*, a homologous protein to *EMILIN1*, was found in higher abundance in the VFLP-ECM when compared to UBM-ECM. However, the information regarding the correlation between EMILIN and TGF-β1 is limited and will be the focus of a future investigation. Interestingly, Dermatopontin and Decorin (*DPT* and *DCN*, respectively) were detected in the VFLP-ECMh. It has been suggested that DPT interacts with *DCN* and modulates TGF-β1 activation [provided by NCBI Gene ID: 1805. RefSeq, Jul 2008]. *CILP-1* was also identified and was recently reported as a modulator of the TGF-β1 pathway in cardiac fibroblasts, among others.[75–76] The mechanism whereby CILP-1 modulates TGF-β1 could be related to thirty cysteines located in the CILP-1 N-terminal associated with binding interaction with TGF-β1.[77] *LTBP4* is part of the TGF-β1 latent activation mechanism and interacts with TGF-β1 leading to modulation in the myofibroblast activation process.[78] The high abundance of *LTBP4* in the VF material revealed new compositional differences that may define the uniqueness of VFLP-ECM compared to UBM-ECM. Even though we have identified this set of proteins with potential TGF-β1 modulating effects, the integrity, and bioactivity after pepsin digestion, and their role within VFLP-ECM during the host tissue response remains to be determined. It is unclear if any of these proteins or fragments are present and active in the final injectable form. However, there is evidence that bioactive peptides and components of the ECM can retain bioactivity even after such manipulation. For example, O'Neil et al. showed that decellularized kidney-ECM sheets had a similar effect on kidney stem cells' metabolic behavior when placed on the papilla ECM when compared to the pepsin digested form of the papilla ECM. These resulted suggested that the digested form retained some of the bioactivity or components recognizable by the kidneys stem cells even after pepsin digestion.[79] Furthermore, Xu et al. identified some of the previously discussed VFLP-ECM proteins as fragments larger than 7 KDa in their derived bovine VF-ECMh with an aligned discussion regarding their potential effect on the TGF-β1 pathway.[80] In summary, the proteomic comparison between the intact VFLP-ECM and UBM-ECM confirmed the distinctive composition of the VFLP-ECM when compared to a commercially available scaffold and highlights potential compositional differences that could reduce myofibroblast activation in vivo.

In vitro modulation of the TGF-β1 pathway by VFLP-ECMh was initially determined via gene expression analysis of HVOX. Previous studies using fat, hyaluronic acid hydrogel, gelatin, growth factors, and cellular components have shown modulation of the scar formation estimated via measurement of either the expression of *ACTA2* or ECM protein expression/deposition.[2, 54, 81–82] VFLP-ECMh was associated with the downregulation of ECM proteins, an important finding as scar formation is the product of aberrant overexpression and deposition of ECM proteins[83–87]. Also, VFLP-ECMh elicited downregulation of *ACTA2* in HVOXs cultured under 2-D and 3-D condition, which is encouraging because overexpression of *ACTA2* has been widely used as a marker of fibroblast activation to myofibroblast[88–91]. Immunostaining for α-SMA and RT-qPCR were fully aligned with transcriptomic outcomes as VFLP-ECMh was not associated with increased expression of *ACTA2* in response to TGF-β1. VFLP-ECMh modulated the TGF-β1 activation pathway, potentially modulating the contractile properties of fibroblasts as well as ECM deposition. Also, an analogous response was found when VFLP-ECMh was tested in a primary cell line human dermal fibroblast (HDFn).

Matrix-Bound Vesicles (MBVs) in the decellularized scaffold were recently postulated as a potential mediator of cell phenotype changes[92]. MBVs are carrier vesicles with a particle size of less than 1000 nm carrying a variety of biomolecules such as miRNA and proteins. MBVs have been isolated from ECM scaffolds (e.g., ECM-hydrogels) and are thought to be responsible for modulating macrophage activation[93–96]. The ultrafiltration approach used in the current study isolated MBVs and potentially other macromolecules larger than 100 kDa during digestion with Collagenase II or Proteinase K. Meanwhile, TCP was the substrate selected to test isolated MBVs as it is stiffer and more likely to elicit myofibroblast activation phenotype as demonstrated in our transcriptomic analysis. *ACTA2* expression was downregulated in response to media supplemented with MBVs and macromolecules. Endostatin, a molecule identified during proteomic analysis, was recently identified in the lumen of the MBVs and found to be, among other important macromolecules involved in the downregulation of *ACTA2*[93]. Future studies will focus on the purification and characterization of the MVBs isolated from VFLP-ECM. However, the data presented provide evidence that the ultrafiltration process of decellularized VFLP-ECM produced bioactive MBVs and macromolecules. Also, supplementation of this extract to media reduced *ACTA2* response associated with TGF-β1 stimulation. These findings provide a foundation for future investigation to compare the effectiveness of the VFLP-ECMh and VFLP-derived MBVs to modulate the fibrotic response *in vivo*.

5. CONCLUSIONS

We derived a VFLP-ECM hydrogel that modulates the expression of various ECM proteins associated with scar formation while downregulating α-SMA (*ACTA2*) associated pathways. Similar responses were observed using macromolecules larger than 100 KDa and MBVs isolated from VFLP-ECM. Cumulatively, these data suggest potential inhibition of fibrosis by VFLP-ECMh via inhibition of TGF-β1 activation.

Supplementary Material

Refer to Web version on PubMed Central for supplementary material.

ACKNOWLEDGEMENTS

We thank our funding sources: National Institutes of Health/National Institute on Deafness and Other Communication Disorders (R01 DC017139-01A1). We also acknowledge the Comparative Medicine Institute (CMI) at NCSU and the Analytical Instrumentation Facility (AIF) at North Carolina State University supported by the State of North Carolina and the National Science Foundation (ECCS-1542015). This work made use of instrumentation at AIF acquired with support from the National Science Foundation (DMR-1726294). The AIF is a member of the North Carolina Research Triangle Nanotechnology Network (RTNN), a site in the National Nanotechnology Coordinated Infrastructure (NNCI). We also thank Dr. Ashley Brown's Lab for their assistance in the AFM measurements. We also acknowledge our undergraduate research assistant Tyler Jordan for his assistance in the MBVs experiments.

REFERENCES

1. Branski RC; Bing R; Kraja I; Amin MR, The role of Smad3 in the fibrotic phenotype in human vocal fold fibroblasts. Laryngoscope 2016, 126 (5), 1151–6. DOI: 10.1002/lary.25673. [PubMed: 26422444]
2. Mattei A; Magalon J; Bertrand B; Philandrianos C; Veran J; Giovanni A, Cell therapy and vocal fold scarring. Eur Ann Otorhinolary 2017, 134 (5), 339–345. DOI: 10.1016/j.anorl.2017.06.006.
3. Mukudai S; Hiwatashi N; Bing R; Garabedian M; Branski RC, Phosphorylation of the glucocorticoid receptor alters SMAD signaling in vocal fold fibroblasts. Laryngoscope 2019, 129 (5), E187–E193. DOI: 10.1002/lary.27570. [PubMed: 30325506]
4. Hiwatashi N; Mukudai S; Bing R; Branski RC, The effects of cytosporone-B, a novel antifibrotic agent, on vocal fold fibroblasts. Laryngoscope 2018, 128 (12), E425–E428. DOI: 10.1002/lary.27361. [PubMed: 30325029]
5. Ramig LO; Verdolini K, Treatment efficacy: voice disorders. Journal of Speech, Language, and Hearing Research 1998, 41 (1), S101–S116.
6. Roy M; Merrill RM; Gray SD; Smith EM, Voice disorders in the general population: prevalence, risk factors, and occupational impact. Laryngoscope 2005, 115 (11), 1988–95. [PubMed: 16319611]
7. Cohen SM; Kim JW; Roy N; Asche C; Courey M, Direct health care costs of laryngeal diseases and disorders. Laryngoscope 2012, 122, 1582–1588. [PubMed: 22544473]
8. Cost of illness summaries for selected conditions. http://www.rti.org/files/COI_Summaries.pdf (accessed September 30).
9. Sullivan PW; Ghushchyan VH; Slejko JF; Belozeroff V; Globe VR; Lin SL, The burden of adult asthma in the United States: evidence from the Medical Expenditure Panel Survey. J Allergy Clin Immunol 2011, 127, 363–369. [PubMed: 21281868]
10. Verdolini K; Ramig LO, Review: occupational risks for voice problems. Logoped Phoniatr Vocol 2001, 26 (1), 37–46. [PubMed: 11432413]
11. Oliveira G; Hirani SP; Epstein R; Yaziqi L; Behlau M, Coping strategies in voice disorders of a Brazilian population. J Voice 2012, 26 (2), 205–213. [PubMed: 21550778]
12. Merrill RM; Anderson AE; Sloan A, Quality of life indicators according to voice disorders and voice-related conditions. Laryngoscope 2011, 121 (9), 2004–2010. [PubMed: 22024857]
13. Catten M; Gray SD; Hammond TH; Zhou RX; Hammond E, Analysis of cellular location and concentration in vocal fold lamina propria. Otolaryng Head Neck 1998, 118 (5), 663–667. DOI: Doi 10.1177/019459989811800516.
14. Falke LL; Gholizadeh S; Goldschmeding R; Kok RJ; Nguyen TQ, Diverse origins of the myofibroblast-implications for kidney fibrosis. Nat Rev Nephrol 2015, 11 (4), 233–44. DOI: 10.1038/nrneph.2014.246. [PubMed: 25584804]
15. Tomasek JJ; Gabbiani G; Hinz B; Chaponnier C; Brown RA, Myofibroblasts and mechano-regulation of connective tissue remodelling. Nat Rev Mol Cell Bio 2002, 3 (5), 349–363. DOI: 10.1038/nrm809. [PubMed: 11988769]

16. Moore J; Thibeault S, Insights Into the Role of Elastin in Vocal Fold Health and Disease. J Voice 2012, 26 (3), 269–275. DOI: 10.1016/j.jvoice.2011.05.003. [PubMed: 21708449]
17. Long JL, Tissue engineering for treatment of vocal fold scar. Curr Opin Otolaryngo 2010, 18 (6), 521–525. DOI: 10.1097/MOO.0b013e32833febf2.
18. King SN; Chen F; Jette ME; Thibeault SL, Vocal fold fibroblasts immunoregulate activated macrophage phenotype. Cytokine 2013, 61 (1), 228–236. DOI: 10.1016/j.cyto.2012.09.023. [PubMed: 23123198]
19. Gray SD; Titze IR; Alipour F; Hammond TH, Biomechanical and histologic observations of vocal fold fibrous proteins. Ann Oto Rhinol Laryn 2000, 109 (1), 77–85. DOI: Doi 10.1177/000348940010900115.
20. Bartlett RS; Thibeault SL; Prestwich GD, Therapeutic potential of gel-based injectables for vocal fold regeneration. Biomed Mater 2012, 7 (2). DOI: Artn 024103 10.1088/1748-6041/7/2/024103.
21. Karajanagi SS; Lopez-Guerra G; Park H; Kobler JB; Galindo M; Aanestad J; Mehta DD; Kumai Y; Giordano N; d'Almeida A; Heaton JT; Langer R; Herrera VL; Faquin W; Hillman RE; Zeitels SM, Assessment of canine vocal fold function after injection of a new biomaterial designed to treat phonatory mucosal scarring. Ann Otol Rhinol Laryngol 2011, 120 (3), 175–84. DOI: 10.1177/000348941112000306. [PubMed: 21510143]
22. Li LQ; Stiadle JM; Lau HK; Zerdoum AB; Jia XQ; Thibeault SL; Kiick KL, Tissue engineering-based therapeutic strategies for vocal fold repair and regeneration. Biomaterials 2016, 108, 91–110. DOI: 10.1016/j.biomaterials.2016.08.054. [PubMed: 27619243]
23. Erndt-Marino JD; Jimenez-Vergara AC; Diaz-Rodriguez P; Kulwatno J; Diaz-Quiroz JF; Thibeault S; Hahn MS, In vitro evaluation of a basic fibroblast growth factor-containing hydrogel toward vocal fold lamina propria scar treatment. J Biomed Mater Res B Appl Biomater 2018, 106 (3), 1258–1267. DOI: 10.1002/jbm.b.33936. [PubMed: 28580765]
24. Gong T; Zhang C; Kang J; Lamb JJ; Jiang JJ, Cryotherapy has antifibrotic and regenerative effects on human vocal fold fibroblasts. Laryngoscope 2019, 129 (4), E143–E150. DOI: 10.1002/lary.27499. [PubMed: 30315572]
25. van den Broek E; Heijnen BJ; Hendriksma M; van de Kamp-Lam VAH; Langeveld APM; van Benthem PPG; Sjogren EV, Bilateral vocal fold injection with autologous fat in patients with vocal fold atrophy with or without sulcus. Eur Arch Otorhinolaryngol 2019, 276 (7), 2007–2013. DOI: 10.1007/s00405-019-05479-5. [PubMed: 31134359]
26. Munger JS; Sheppard D, Cross talk among TGF-beta signaling pathways, integrins, and the extracellular matrix. Cold Spring Harb Perspect Biol 2011, 3 (11), a005017. DOI: 10.1101/cshperspect.a005017. [PubMed: 21900405]
27. Wrona EA; Peng R; Amin MR; Branski RC; Freytes DO, Extracellular Matrix for Vocal Fold Lamina Propria Replacement: A Review. Tissue Eng Part B-Re 2016, 22 (6), 421–429. DOI: 10.1089/ten.teb.2016.0015.
28. Badylak SF; Freytes DO; Gilbert TW, Extracellular matrix as a biological scaffold material: Structure and function. Acta Biomater 2009, 5 (1), 1–13. DOI: 10.1016/j.actbio.2008.09.013. [PubMed: 18938117]
29. Saldin LT; Cramer MC; Velankar SS; White LJ; Badylak SF, Extracellular matrix hydrogels from decellularized tissues: Structure and function. Acta Biomater 2017, 49, 1–15. DOI: 10.1016/j.actbio.2016.11.068. [PubMed: 27915024]
30. Wang RM; Christman KL, Decellularized myocardial matrix hydrogels: In basic research and preclinical studies. Adv Drug Deliv Rev 2016, 96, 77–82. DOI: 10.1016/j.addr.2015.06.002. [PubMed: 26056717]
31. Gilbert TW; Stolz DB; Biancaniello F; Simmons-Byrd A; Badylak SF, Production and characterization of ECM powder: implications for tissue engineering applications. Biomaterials 2005, 26 (12), 1431–1435. DOI: 10.1016/j.biomaterials.2004.04.042. [PubMed: 15482831]
32. Gaffney L; Wrona EA; Freytes DO, Potential Synergistic Effects of Stem Cells and Extracellular Matrix Scaffolds. Acs Biomater Sci Eng 2018, 4 (4), 1208–1222. DOI: 10.1021/acsbiomaterials.7b00083.

33. Brown BN; Ratner BD; Goodman SB; Amar S; Badylak SF, Macrophage polarization: an opportunity for improved outcomes in biomaterials and regenerative medicine. Biomaterials 2012, 33 (15), 3792–802. DOI: 10.1016/j.biomaterials.2012.02.034. [PubMed: 22386919]
34. Dearth CL; Slivka PF; Stewart SA; Keane TJ; Tay JK; Londono R; Goh Q; Pizza FX; Badylak SF, Inhibition of COX1/2 alters the host response and reduces ECM scaffold mediated constructive tissue remodeling in a rodent model of skeletal muscle injury. Acta Biomater 2016, 31, 50–60. DOI: 10.1016/j.actbio.2015.11.043. [PubMed: 26612417]
35. Freytes DO; Martin J; Velankar SS; Lee AS; Badylak SF, Preparation and rheological characterization of a gel form of the porcine urinary bladder matrix. Biomaterials 2008, 29 (11), 1630–7. DOI: 10.1016/j.biomaterials.2007.12.014. [PubMed: 18201760]
36. Traverse JH; Henry TD; Dib N; Patel AN; Pepine C; Schaer GL; DeQuach JA; Kinsey AM; Chamberlin P; Christman KL, First-in-Man Study of a Cardiac Extracellular Matrix Hydrogel in Early and Late Myocardial Infarction Patients. JACC: Basic to Translational Science 2019, 357. DOI: 10.1016/j.jacbts.2019.07.012.
37. Wrona EA; Peng R; Born H; Amin MR; Branski RC; Freytes DO, Derivation and characterization of porcine vocal fold extracellular matrix scaffold. Laryngoscope 2016, 126 (4), 928–35. DOI: 10.1002/lary.25640. [PubMed: 26371887]
38. Nolan T; Hands RE; Bustin SA, Quantification of mRNA using real-time RT-PCR. Nature Protocols 2006, 1 (3), 1559–1582. DOI: 10.1038/nprot.2006.236. [PubMed: 17406449]
39. Dobin A; Davis CA; Schlesinger F; Drenkow J; Zaleski C; Jha S; Batut P; Chaisson M; Gingeras TR, STAR: ultrafast universal RNA-seq aligner. Bioinformatics 2013, 29 (1), 15–21. DOI: 10.1093/bioinformatics/bts635bts635 [pii]. [PubMed: 23104886]
40. Law CW; Chen Y; Shi W; Smyth GK, voom: Precision weights unlock linear model analysis tools for RNA-seq read counts. Genome Biol 2014, 15 (2), R29. DOI: 10.1186/gb-2014-15-2-r29. [PubMed: 24485249]
41. Ritchie ME; Phipson B; Wu D; Hu Y; Law CW; Shi W; Smyth GK, limma powers differential expression analyses for RNA-sequencing and microarray studies. Nucleic Acids Res 2015, 43 (7), e47. DOI: 10.1093/nar/gkv007. [PubMed: 25605792]
42. Benjamini Y; Hochberg Y, Controlling the false discovery rate: a practical and powerful approach to multiple testing. J.Roy.Statist.Soc.Ser 1995, B (57), 289–300.
43. Tyanova S; Temu T; Sinitcyn P; Carlson A; Hein MY; Geiger T; Mann M; Cox J, The Perseus computational platform for comprehensive analysis of (prote)omics data. Nat Methods 2016, 13 (9), 731–40. DOI: 10.1038/nmeth.3901. [PubMed: 27348712]
44. Yu LL; Zhu J; Liu JX; Jiang F; Ni WK; Qu LS; Ni RZ; Lu CH; Xiao MB, A Comparison of Traditional and Novel Methods for the Separation of Exosomes from Human Samples. Biomed Res Int 2018, 2018, 3634563. DOI: 10.1155/2018/3634563. [PubMed: 30148165]
45. Vandergriff AC; de Andrade JB; Tang J; Hensley MT; Piedrahita JA; Caranasos TG; Cheng K, Intravenous Cardiac Stem Cell-Derived Exosomes Ameliorate Cardiac Dysfunction in Doxorubicin Induced Dilated Cardiomyopathy. Stem Cells Int 2015, 2015, 960926. DOI: 10.1155/2015/960926. [PubMed: 26351465]
46. Cappione A GS, Mabuchi M, Smith J, Strug I, Nadler T A Centrifugal Ultrafiltration-Based Method for Enrichment of Microvesicles; 2014.
47. Svistushkin MV; Kotova SL; Shekhter AB; Svistushkin VM; Akovantseva AA; Frolova AA; Fayzullin AL; Starostina SV; Bezrukov EA; Sukhanov RB; Timashev SF; Butnaru DV; Timashev PS, Collagen fibrillar structures in vocal fold scarring and repair using stem cell therapy: a detailed histological, immunohistochemical and atomic force microscopy study. J Microsc 2019, 274 (1), 55–68. DOI: 10.1111/jmi.12784. [PubMed: 30740689]
48. Latifi N; Asgari M; Vali H; Mongeau L, A tissue-mimetic nano-fibrillar hybrid injectable hydrogel for potential soft tissue engineering applications. Sci Rep-Uk 2018, 8. DOI: ARTN 1047 10.1038/s41598-017-18523-3.
49. Duan Y; Liu Z; O'Neill J; Wan LQ; Freytes DO; Vunjak-Novakovic G, Hybrid gel composed of native heart matrix and collagen induces cardiac differentiation of human embryonic stem cells without supplemental growth factors. J Cardiovasc Transl Res 2011, 4 (5), 605–15. DOI: 10.1007/s12265-011-9304-0. [PubMed: 21744185]

50. Chan RW; Titze IR, Viscosities of Implantable Biomaterials in Vocal Fold Augmentation Surgery. The Laryngoscope 1998, 108 (5), 725–731. DOI: 10.1097/00005537-199805000-00019. [PubMed: 9591554]
51. Wassenaar JW; Braden RL; Osborn KG; Christman KL, Modulating In Vivo Degradation Rate of Injectable Extracellular Matrix Hydrogels. J Mater Chem B 2016, 4 (16), 2794–2802. DOI: 10.1039/C5TB02564H. [PubMed: 27563436]
52. Spang MT; Christman KL, Extracellular matrix hydrogel therapies: In vivo applications and development. Acta Biomater 2018, 68, 1–14. DOI: 10.1016/j.actbio.2017.12.019. [PubMed: 29274480]
53. Chester D; Kathard R; Nortey J; Nellenbach K; Brown AC, Viscoelastic properties of microgel thin films control fibroblast modes of migration and pro-fibrotic responses. Biomaterials 2018, 185, 371–382. DOI: 10.1016/j.biomaterials.2018.09.012. [PubMed: 30292092]
54. Hiwatashi N; Bing R; Kraja I; Branski RC, Mesenchymal Stem Cells Have Antifibrotic Effects on Transforming Growth Factor-beta 1-Stimulated Vocal Fold Fibroblasts. Laryngoscope 2017, 127 (1), E35–E41. DOI: 10.1002/lary.26121. [PubMed: 27345475]
55. Hiwatashi N; Bing R; Kraja I; Branski RC, NR4A1 is an endogenous inhibitor of vocal fold fibrosis. Laryngoscope 2017, 127 (9), E317–E323. DOI: 10.1002/lary.26678. [PubMed: 28581197]
56. Zeitels SMN, MA, US), Hillman Robert Edward (Weston, MA, US), Karajanagi Sandeep Sidram (Malden, MA, US), Langer Robert S. (Newton, MA, US) HYDROGELS FOR VOCAL CORD AND SOFT TISSUE AUGMENTATION AND REPAIR. 2010.
57. Kwon SK; Kim HB; Song JJ; Cho CG; Park SW; Choi JS; Ryu J; Oh SH; Lee JH, Vocal Fold Augmentation with Injectable Polycaprolactone Microspheres/Pluronic F127 Hydrogel: Long-Term In Vivo Study for the Treatment of Glottal Insufficiency. Plos One 2014, 9 (1). DOI: ARTN e85512 10.1371/journal.pone.0085512.
58. Lasso José M., P. D, 2 Scola Batolomé,2 Gómez-Vilda Pedro,3 García-Martín Ana I.,4 and Fernández-Santos María Eugenia5, Injection Laryngoplasty Using Autologous Fat Enriched with Adipose-Derived Regenerative Stem Cells: A Safe Therapeutic Option for the Functional Reconstruction of the Glottal Gap after Unilateral Vocal Fold Paralysis. Stem Cells International 2018, 2018, 15. DOI: 10.1155/2018/8917913.
59. Li L; Stiadle JM; Lau HK; Zerdoum AB; Jia X; Thibeault SL; Kiick KL, Tissue engineering-based therapeutic strategies for vocal fold repair and regeneration. Biomaterials 2016, 108, 91–110. DOI: 10.1016/j.biomaterials.2016.08.054. [PubMed: 27619243]
60. Bartlett RS; Thibeault SL; Prestwich GD, Therapeutic potential of gel-based injectables for vocal fold regeneration. Biomed Mater 2012, 7 (2), 024103. DOI: 10.1088/1748-6041/7/2/024103. [PubMed: 22456756]
61. Karajanagi SS; Lopez-Guerra G; Park H; Kobler JB; Galindo M; Aanestad J; Mehta DD; Kumai Y; Giordano N; d'Almeida A; Heaton JT; Langer R; Herrera VL; Faquin W; Hillman RE; Zeitels SM, Assessment of Canine Vocal Fold Function After Injection of a New Biomaterial Designated to Treat Phonatory Mucosal Scarring. Ann Otol Rhinol Laryngol 2011, 120 (3), 175–184. [PubMed: 21510143]
62. Huber JE; Spievack A; Simmons-Byrd A; Ringel RL; Badylak S, Extracellular matrix as a scaffold for laryngeal reconstruction. Ann Otol Rhinol Laryngol 2003, 112 (5), 428–33. [PubMed: 12784982]
63. Ringel RL; Kahane JC; Hillsamer PJ; Lee AS; Badylak SF, The application of tissue engineering procedures to repair the larynx J Speech Lang Hear Res 2006, 49, 194–208. [PubMed: 16533084]
64. Alcaraz J; Otero J; Jorba I; Navajas D, Bidirectional mechanobiology between cells and their local extracellular matrix probed by atomic force microscopy. Semin Cell Dev Biol 2018, 73, 71–81. DOI: 10.1016/j.semcdb.2017.07.020. [PubMed: 28743639]
65. Franke K; Sapudom J; Kalbitzer L; Anderegg U; Pompe T, Topologically defined composites of collagen types I and V as in vitro cell culture scaffolds. Acta Biomater 2014, 10 (6), 2693–702. DOI: 10.1016/j.actbio.2014.02.036. [PubMed: 24590159]
66. Achterberg VF; Buscemi L; Diekmann H; Smith-Clerc J; Schwengler H; Meister JJ; Wenck H; Gallinat S; Hinz B, The Nano-Scale Mechanical Properties of the Extracellular Matrix Regulate

Dermal Fibroblast Function. Journal of Investigative Dermatology 2014, 134 (7), 1862–1872. DOI: 10.1038/jid.2014.90.

67. Kazemirad S; Heris HK; Mongeau L, Viscoelasticity of hyaluronic acid-gelatin hydrogels for vocal fold tissue engineering. J Biomed Mater Res B 2016, 104 (2), 283–290. DOI: 10.1002/jbm.b.33358.
68. Davis GE; Bayless KJ; Davis MJ; Meininger GA, Regulation of tissue injury responses by the exposure of matricryptic sites within extracellular matrix molecules. Am J Pathol 2000, 156 (5), 1489–98. DOI: 10.1016/S0002-9440(10)65020-1. [PubMed: 10793060]
69. Karsdal MA, Biochemistry of Collagens, Laminins and Elastin Structure, Function and Biomarkers Introduction. Biochemistry of Collagens, Laminins and Elastin: Structure, Function and Biomarkers 2016, Xix–Xxxiv.
70. Schiavinato A; Keene DR; Imhof T; Doliana R; Sasaki T; Sengle G, Fibulin-4 deposition requires EMILIN-1 in the extracellular matrix of osteoblasts. Sci Rep-Uk 2017, 7. DOI: ARTN 5526 10.1038/s41598-017-05835-7.
71. Naba A; Clauser KR; Mani DR; Carr SA; Hynes RO, Quantitative proteomic profiling of the extracellular matrix of pancreatic islets during the angiogenic switch and insulinoma progression. Sci Rep-Uk 2017, 7. DOI: ARTN 40495 10.1038/srep40495.
72. Munger JS; Sheppard D, Cross Talk among TGF-beta Signaling Pathways, Integrins, and the Extracellular Matrix. Csh Perspect Biol 2011, 3 (11). DOI: ARTN a005017 10.1101/cshperspect.a005017.
73. Mayorca-Guiliani AE; Madsen CD; Cox TR; Horton ER; Venning FA; Erler JT, ISDoT: in situ decellularization of tissues for high-resolution imaging and proteomic analysis of native extracellular matrix. Nat Med 2017, 23 (7), 890-+. DOI: 10.1038/nm.4352. [PubMed: 28604702]
74. Ling CY; Li QY; Brown ME; Kishimoto Y; Toya Y; Devine EE; Choi KO; Nishimoto K; Norman IG; Tsegyal T; Jiang JJ; Burlingham WJ; Gunasekaran S; Smith LM; Frey BL; Welham NV, Bioengineered vocal fold mucosa for voice restoration. Sci Transl Med 2015, 7 (314). DOI: ARTN 314ra187 10.1126/scitranslmed.aab4014.
75. Shindo K; Asakura M; Min KD; Ito S; Fu HY; Yamazaki S; Takahashi A; Imazu M; Fukuda H; Nakajima Y; Asanuma H; Minamino T; Takashima S; Minamino N; Mochizuki N; Kitakaze M, Cartilage Intermediate Layer Protein 1 Suppresses TGF-beta Signaling in Cardiac Fibroblasts. Int J Gerontol 2017, 11 (2), 67–74. DOI: 10.1016/j.ijge.2017.01.002.
76. Bernardo BC; Belluoccio D; Rowley L; Little CB; Hansen U; Bateman JF, Cartilage Intermediate Layer Protein 2 (CILP-2) Is Expressed in Articular and Meniscal Cartilage and Down-regulated in Experimental Osteoarthritis. Journal of Biological Chemistry 2011, 286 (43), 37758–37767. DOI: 10.1074/jbc.M111.248039.
77. Mori M; Nakajima M; Mikami Y; Seki S; Takigawa M; Kubo T; Ikegawa S, Transcriptional regulation of the cartilage intermediate layer protein (CILP) gene. Biochem Bioph Res Co 2006, 341 (1), 121–127. DOI: 10.1016/j.bbrc.2005.12.159.
78. Hinz B, Tissue stiffness, latent TGF-beta1 activation, and mechanical signal transduction: implications for the pathogenesis and treatment of fibrosis. Curr Rheumatol Rep 2009, 11 (2), 120–6. [PubMed: 19296884]
79. O'Neill JD; Freytes DO; Anandappa AJ; Oliver JA; Vunjak-Novakovic GV, The regulation of growth and metabolism of kidney stem cells with regional specificity using extracellular matrix derived from kidney. Biomaterials 2013, 34 (38), 9830–41. DOI: 10.1016/j.biomaterials.2013.09.022. [PubMed: 24074840]
80. Xu CC; Mau T, A tissue-specific, injectable acellular gel for the treatment of chronic vocal fold scarring. Acta Biomater 2019. DOI: 10.1016/j.actbio.2019.08.025.
81. Kumai Y; Kobler JB; Park H; Galindo M; Herrera VLM; Zeitels SM, Modulation of Vocal Fold Scar Fibroblasts By Adipose-Derived Stem/Stromal Cells. Laryngoscope 2010, 120 (2), 330–337. DOI: 10.1002/lary.20753. [PubMed: 20013848]
82. Kishimoto Y; Hirano S; Kitani Y; Suehiro A; Umeda H; Tateya I; Kanemaru S; Tabata Y; Ito J, Chronic Vocal Fold Scar Restoration With Hepatocyte Growth Factor Hydrogel. Laryngoscope 2010, 120 (1), 108–113. DOI: 10.1002/lary.20642. [PubMed: 19877197]

83. Scharenberg MA; Pippenger BE; Sack R; Zingg D; Ferralli J; Schenk S; Martin I; Chiquet-Ehrismann R, TGF- -induced differentiation into myofibroblasts involves specific regulation of two MKL1 isoforms. Journal of Cell Science 2014, 127 (5), 1079–1091. DOI: 10.1242/jcs.142075. [PubMed: 24424023]
84. Mebarki S; Désert R; Sulpice L; Sicard M; Desille M; Canal F; Dubois-Pot Schneider H; Bergeat D; Turlin B; Bellaud P; Lavergne E; Le Guével R; Corlu A; Perret C; Coulouarn C; Clément B; Musso O, De novo HAPLN1 expression hallmarks Wnt-induced stem cell and fibrogenic networks leading to aggressive human hepatocellular carcinomas. Oncotarget 2016, 7 (26), 39026–39043. DOI: 10.18632/oncotarget.9346. [PubMed: 27191501]
85. Karbiener M; Darnhofer B; Frisch MT; Rinner B; Birner-Gruenberger R; Gugatschka M, Comparative proteomics of paired vocal fold and oral mucosa fibroblasts. Journal of Proteomics 2017, 155, 11–21. DOI: 10.1016/j.jprot.2017.01.010. [PubMed: 28099887]
86. Herum K; Lunde I; McCulloch A; Christensen G, The Soft- and Hard-Heartedness of Cardiac Fibroblasts: Mechanotransduction Signaling Pathways in Fibrosis of the Heart. Journal of Clinical Medicine 2017, 6 (5), 53–53. DOI: 10.3390/jcm6050053.
87. Achterberg VF; Buscemi L; Diekmann H; Smith-Clerc J; Schwengler H; Meister J-J; Wenck H; Gallinat S; Hinz B, The Nano-Scale Mechanical Properties of the Extracellular Matrix Regulate Dermal Fibroblast Function. Journal of Investigative Dermatology 2014, 134 (7), 1862–1872. DOI: 10.1038/jid.2014.90.
88. Herum KM; Lunde IG; McCulloch AD; Christensen G, The Soft-and Hard-Heartedness of Cardiac Fibroblasts: Mechanotransduction Signaling Pathways in Fibrosis of the Heart. Journal of Clinical Medicine 2017, 6 (5). DOI: ARTN 53 10.3390/jcm6050053.
89. Kaur H; Carvalho J; Looso M; Singh P; Chennupati R; Preussner J; Gunther S; Albarran-Juarez J; Tischner D; Classen S; Offermanns S; Wettschureck N, Single-cell profiling reveals heterogeneity and functional patterning of GPCR expression in the vascular system. Nat Commun 2017, 8. DOI: ARTN 15700 10.1038/ncomms15700.
90. Kishimoto Y; Kishimoto AO; Ye SY; Kendziorski C; Welham NV, Modeling fibrosis using fibroblasts isolated from scarred rat vocal folds. Laboratory Investigation 2016, 96 (7), 807–816. DOI: 10.1038/labinvest.2016.43. [PubMed: 27111284]
91. Scharenberg MA; Pippenger BE; Sack R; Zingg D; Ferralli J; Schenk S; Martin I; Chiquet-Ehrismann R, TGF-beta-induced differentiation into myofibroblasts involves specific regulation of two MKL1 isoforms. Journal of Cell Science 2014, 127 (5), 1079–1091. DOI: 10.1242/jcs.142075. [PubMed: 24424023]
92. Huleihel L; Hussey GS; Naranjo JD; Zhang L; Dziki JL; Turner NJ; Stolz DB; Badylak SF, Matrix-bound nanovesicles within ECM bioscaffolds. Sci Adv 2016, 2 (6). DOI: UNSP e1600502 10.1126/sciadv.1600502.
93. Hussey GS; Dziki JL; Lee YC; Bartolacci JG; Behun M; Turnquist HR; Badylak SF, Matrix bound nanovesicle-associated IL-33 activates a pro-remodeling macrophage phenotype via a non-canonical, ST2-independent pathway. Journal of Immunology and Regenerative Medicine 2019, 3, 26–35. DOI: 10.1016/j.regen.2019.01.001. [PubMed: 31656879]
94. Huleihel L; Bartolacci JG; Dziki JL; Vorobyov T; Arnold B; Scarritt ME; Molina CP; LoPresti ST; Brown BN; Naranjo JD; Badylak SF, Matrix-Bound Nanovesicles Recapitulate Extracellular Matrix Effects on Macrophage Phenotype. Tissue Eng Pt A 2017, 23 (21–22), 1283–1294. DOI: 10.1089/ten.tea.2017.0102.
95. Dziki J; Huleihel L; Bartolacci J; Vorobyov T; Arnold B; Scarritt M; Pineda C; LoPresti S; Brown B; Badylak S, Matrix-bound Nanovesicles Recapitulate the Effects of ECM Bioscaffolds upon Macrophage Phenotype. Tissue Eng Pt A 2017, 23, S35–S35.
96. Bartolacci J; Badylak S, Matrix-bound Nanovesicles Within Tissue ECM Rapidly Alter Their Cargo In Response To Tissue Injury In A Rat Muscle Crush Model. Tissue Eng Pt A 2017, 23, S68–S68.

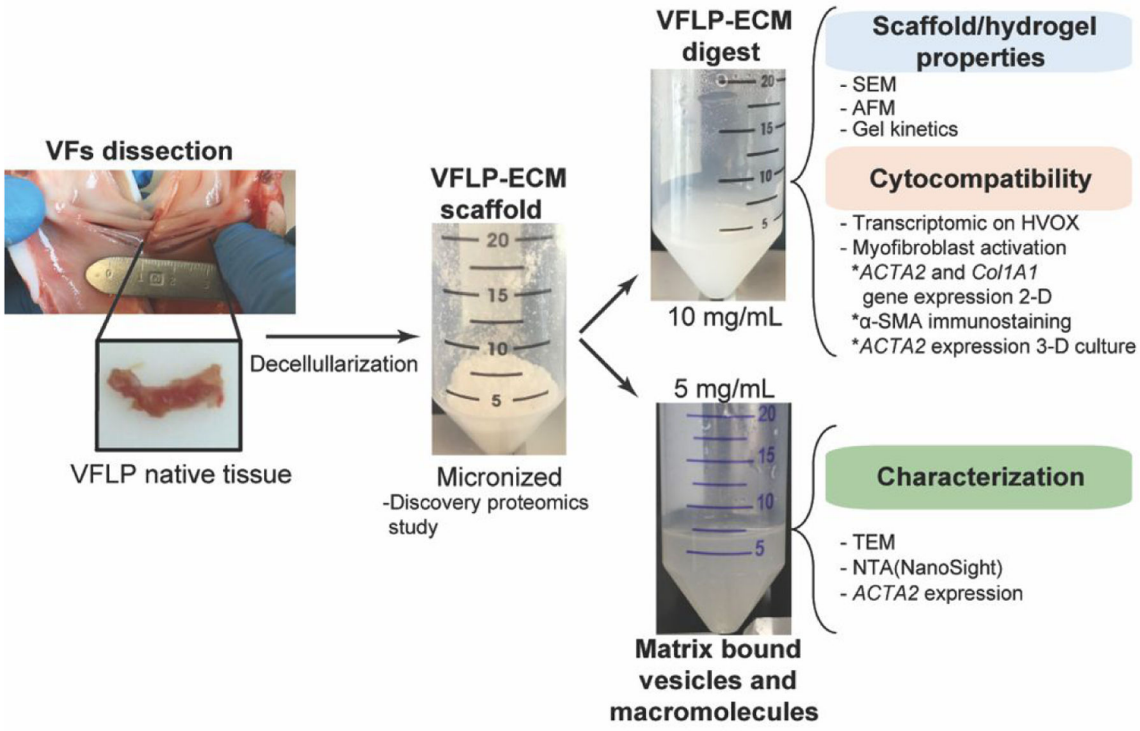

Figure 1.
General approach employed to characterize the derived decellularized VFLP-ECMh and its precursor.

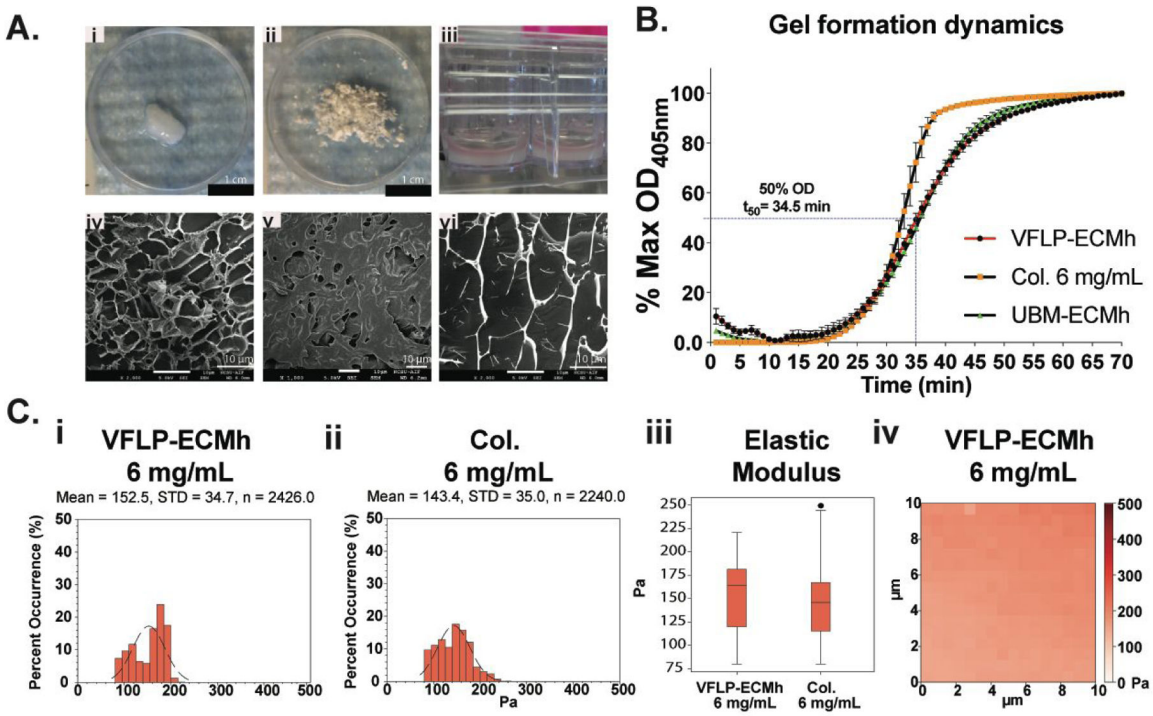

Figure 2. VFLP-ECM scaffolds Properties.

VFLP-ECM scaffold characterization. Collagen type I hydrogel was represented in the figures with Col. A) Macro and Microphotographs of the decellularized VFLP (i and iv), micronized VFLP-ECM (ii and v), and VFLP-ECMh (iii and vi). B) Gel kinetics based on absorbance for VFLP-ECMh compared to Collagen Type I, and UBM-ECMh. Error bars represent the SEM of at least three independent experiments with each condition being measured in triplicate. Plots C) i-iii represent the local surface modulus of the different hydrogels determined via Atomic Force Microscopy (AFM) in contact force mode. iv) Representative force map for the VFLP-ECMh at 6 mg mL^{-1}.

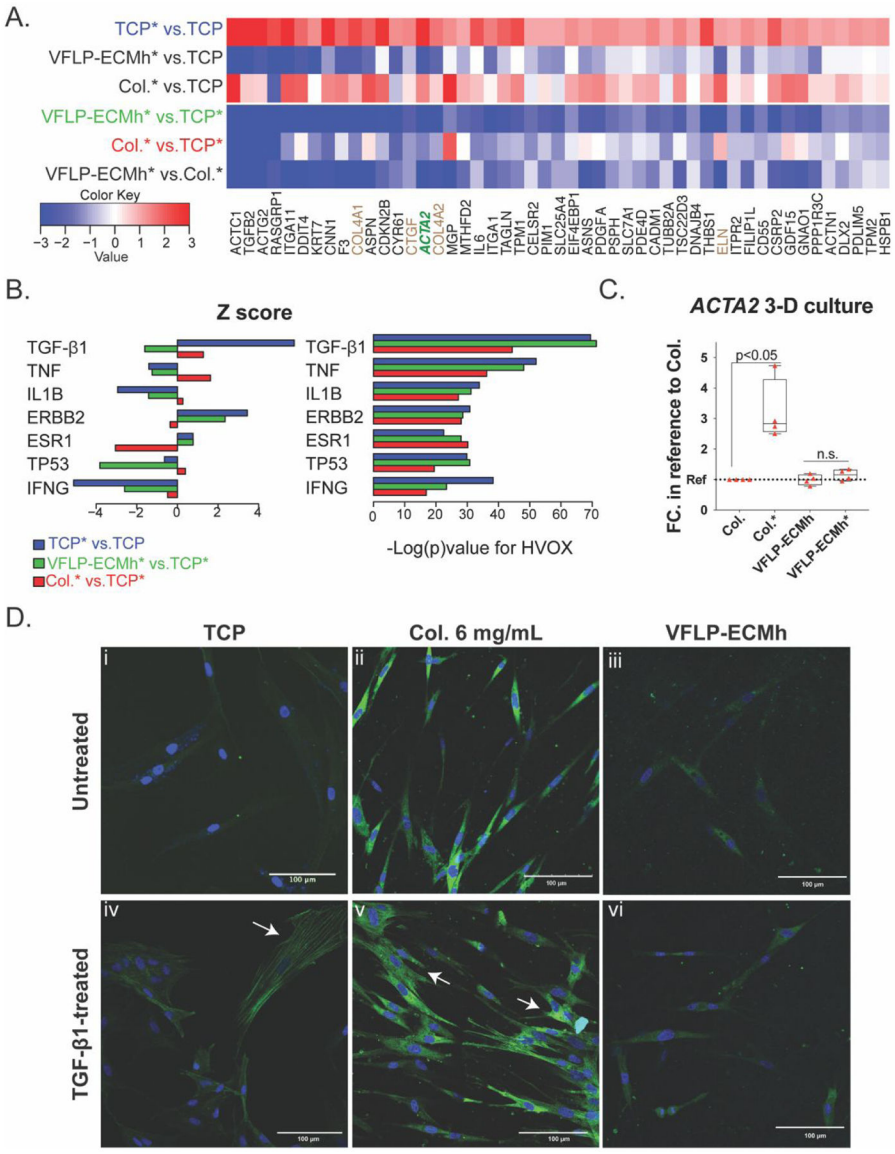

Figure 3. Transcriptomics, *ACTA2* RT-qPCR in 3-D culture, and α-SMA immunostaining.

Transcriptome deep sequencing (RNA-seq) of HVOX cultured on TCP, VFLP-ECMh, and Col. unstimulated or stimulated with TGF-β1. Collagen Type I hydrogel was represented with Col., and TGF-β1 treatment was represented in the figure with the symbol "*" next to the material tested. A. Heatmap showing a subset of genes manually selected from those genes that: 1) significantly up-regulated in HVOX growing on TCP*; 2) exhibited significant difference between VFLP-ECMh* vs. TCP* (Green) comparison; 3) were annotated TGF-β1 targets provided by Ingenuity Pathway Analysis; 4) were down-regulated by VFLP-ECMh on both HVOX and human dermal fibroblast HDFn (Figure A3iii). The brown font color used for some of the gene names in the heat map is to highlight an extracellular matrix related gene or the green font color used for *ACTA2* because it represents an important marker for myofibroblast activation. B). Bar plots of predicted gene expression regulators based on targets enriched in the differentially expressed genes in HVOX for each of the three

comparisons: TCP* vs. TCP (Blue bars), VFLP-ECMh* vs. TCP* (Green bars), Col.* vs. TCP* (Red bars). Only the top 5 regulators with the most significant enrichment p-values in any of the three comparisons were shown. Left: target activation z-score. Right: enrichment p-value. C) *ACTA2* expression in HVOX cultured in 3-D in Col. or VFLP-ECMh treated or untreated with TGF-β1. D) α-SMA immunostaining in HVOX cultured on TCP, Col., and VFLP-ECMh (Green=α-SMA, blue= DAPI). Figure A3 TCP and Col. 4 mg/mL were used as positive controls.

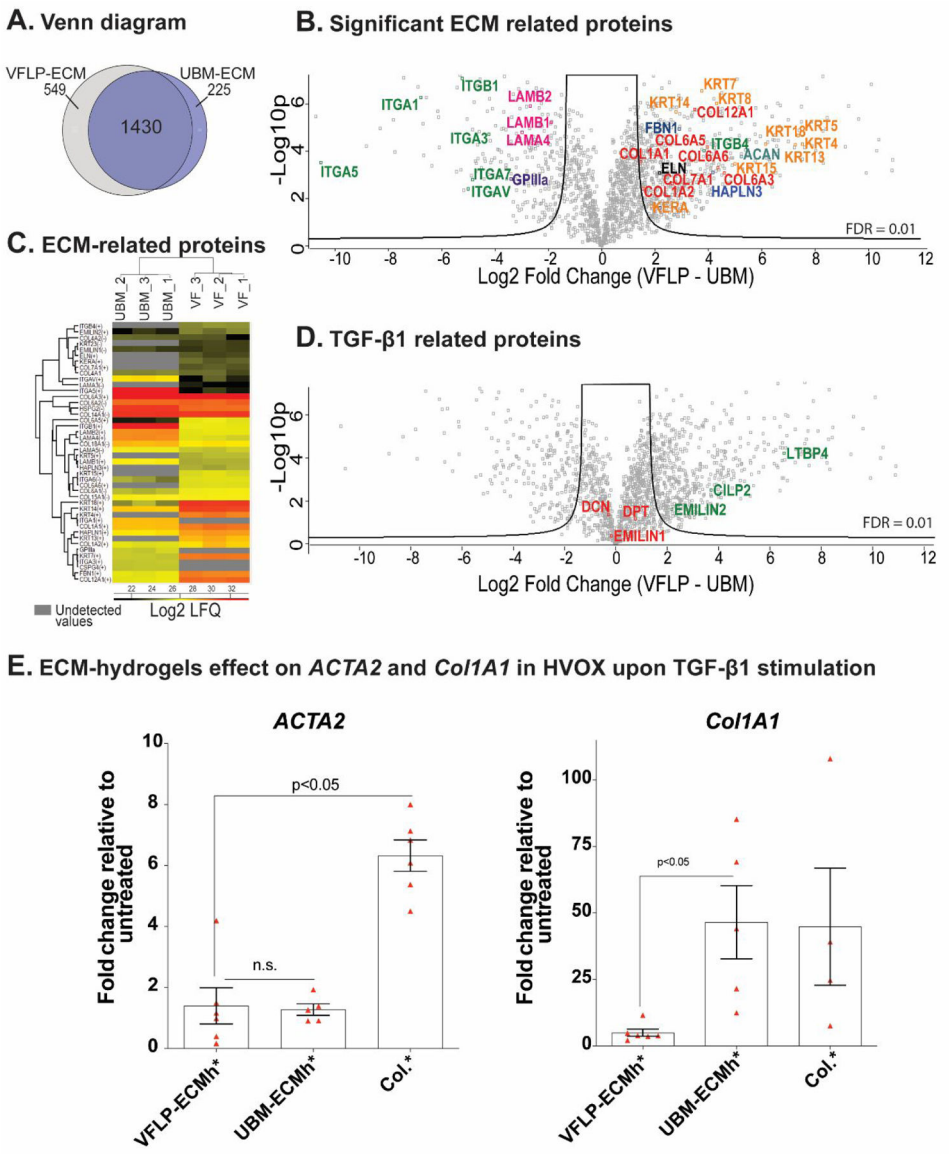

Figure 4. Proteomics and ECM- effect on *ACTA2* and *Col1A1* expression.

Discovery proteomics for VFLP-ECM and UBM-ECM. A) Venn diagram grouping and contrasting the total number of proteins detected and identified for each biomaterial. B) Volcano plot representing the significant ECM related proteins (gene name nomenclature) after Perseus analysis. Proteins displayed were detected in at least two independent replicates in either VFLP or UBM ECM. C) Heat map for the entire set of ECM related proteins detected in either scaffold. The (+) or (−) symbol next to the gene name indicates if the protein was or was not significant in the relative quantification between VFLP and UBM ECM. D) Volcano plot showing the proteins related to the TGF-β1 pathway. E) Fold Change of *ACTA2* and *Col1A1* in reference to TGF-β1 untreated. Error bars represent SEM. UBM-ECMh condition treated and untreated had a p-value <0.05 for *ACTA2* analyzed by t-test paired with at least n=5.

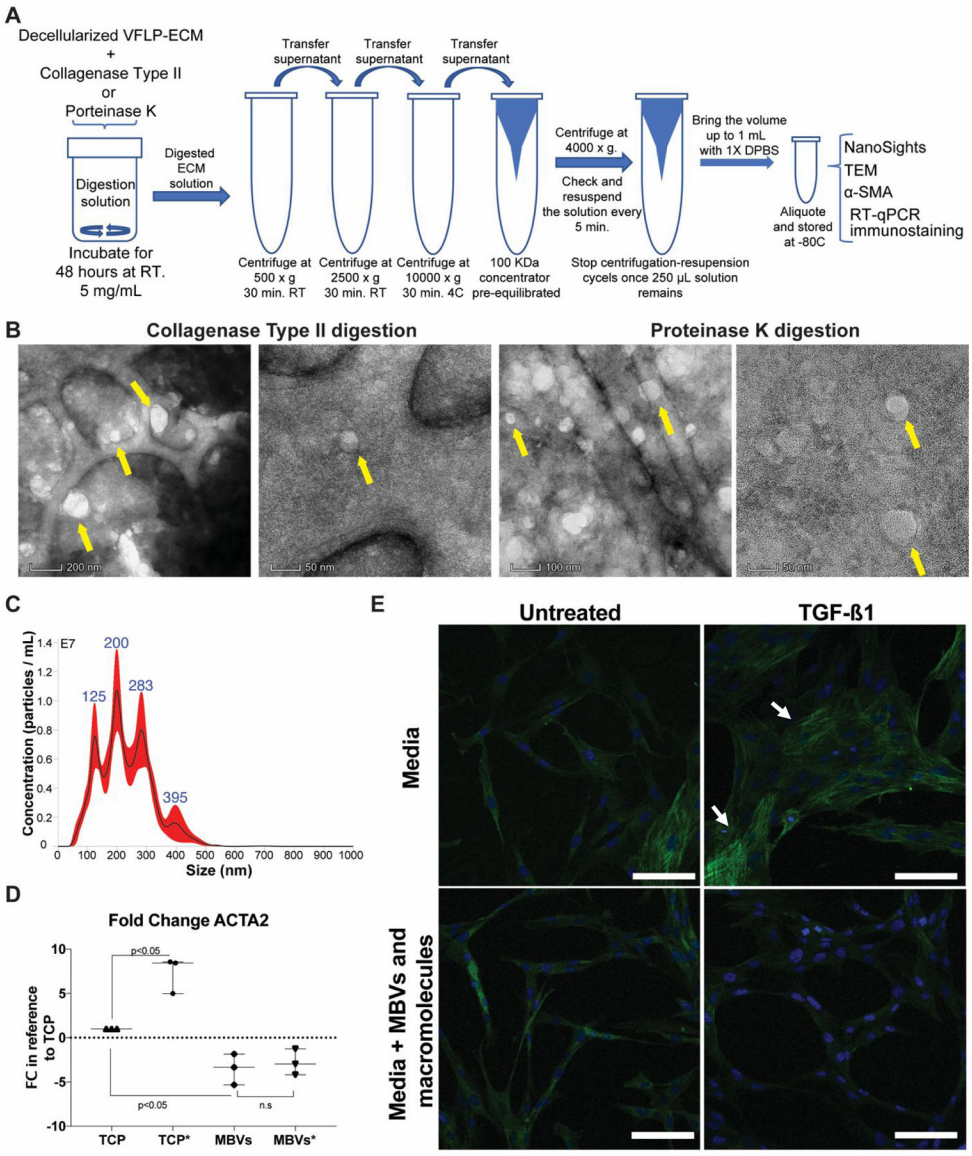

Figure 5. MBVs and macromolecules isolation and concentration from the digestion of decellularized VFLP-ECM and α-SMA immunostaining.

MBVs and macromolecules isolation and characterization from acellularized VFLP-ECM. A) General sketch used to isolate and concentrate MBVs from digested VFLP-ECM using an ultrafiltration approach. B) Representative Transmission Electron Microscopy (TEM) images of the digested product, either by Collagenase Type II or Proteinase K treatment. The samples after ultrafiltration and concentration were negative stained using Uranyl Acetate. C) Nanoparticle Tracking Analysis (NTA) using NanoSight. D) *ACTA2* Fold Change (FC) in reference to the basal expression of cells growing on TCP with no treatment. The control cells were compared with cells supplemented with the ultrafiltrated product at a concentration of approximately 25×10^6 particles mL^{-1}, treated or untreated with TGF-β1 at 10 ng mL^{-1} for 48 hours. E) Confocal images are showing α-SMA immunostaining for each condition (scale bar 100 µm).

Table 1.

Label-Free Quantification for proteins related to the TGF-β1 pathway

	VFLP-ECM			UBM-ECM		
GENE ID	**LFQ-1**	**LFQ-2**	**LFQ-3**	**LFQ-1**	**LFQ-2**	**LFQ-3**
DPT	30.7465	30.4921	31.4469	30.3023	29.9805	30.1410
DCN	32.4232	32.6477	32.7102	32.9827	32.8195	32.8613
EMILIN1	23.2633	23.3852	23.0247	23.0838	23.5174	23.5984
EMILIN2	24.6314	24.1147	24.5666	22.5214	21.1211	23.1405
LTBP4	27.5538	27.5130	27.8912	21.7539	20.9829	20.5546
CILP2	24.9115	24.5792	24.7704	20.2897	20.7014	22.1778

The values represent the Log2 for the label-free quantification (LFQ) intensity measured per sample.